Gene editing of hematopoietic stem cells restores T-cell response in familial hemophagocytic lymphohistiocytosis

Viviane Dettmer-Monaco, PhD,[a,b]* Kristoffer Weißert, PhD,[b,c]* Sandra Ammann, PhD,[b,c] Gianni Monaco, PhD,[a,b,d] Lei Lei, MSc,[a,b,e] Linda Gräßel, MD,[f,g] Manuel Rhiel, PhD,[a,b] Julia Rositzka, MSc,[a,b] Masako M. Kaufmann, MSc,[a,b,h] Kerstin Geiger, MSc,[a,b,e] Geoffroy Andrieux, PhD,[i,j] Jessica Lao, MSc,[b,c,e] Gudrun Thoulass, MSc,[b,c,e] Christoph Schell, MD, PhD,[j,k] Melanie Boerries, MD, PhD,[g,i,j] Anna L. Illert, MD,[f,g,j]§ Tatjana I. Cornu, PhD,[a,b,j] Stephan Ehl, MD,[b,c,j] Peter Aichele, PhD,[b,c,j]‡ and Toni Cathomen, PhD[a,b,j]‡ *Freiburg and Heidelberg, Germany*

GRAPHICAL ABSTRACT

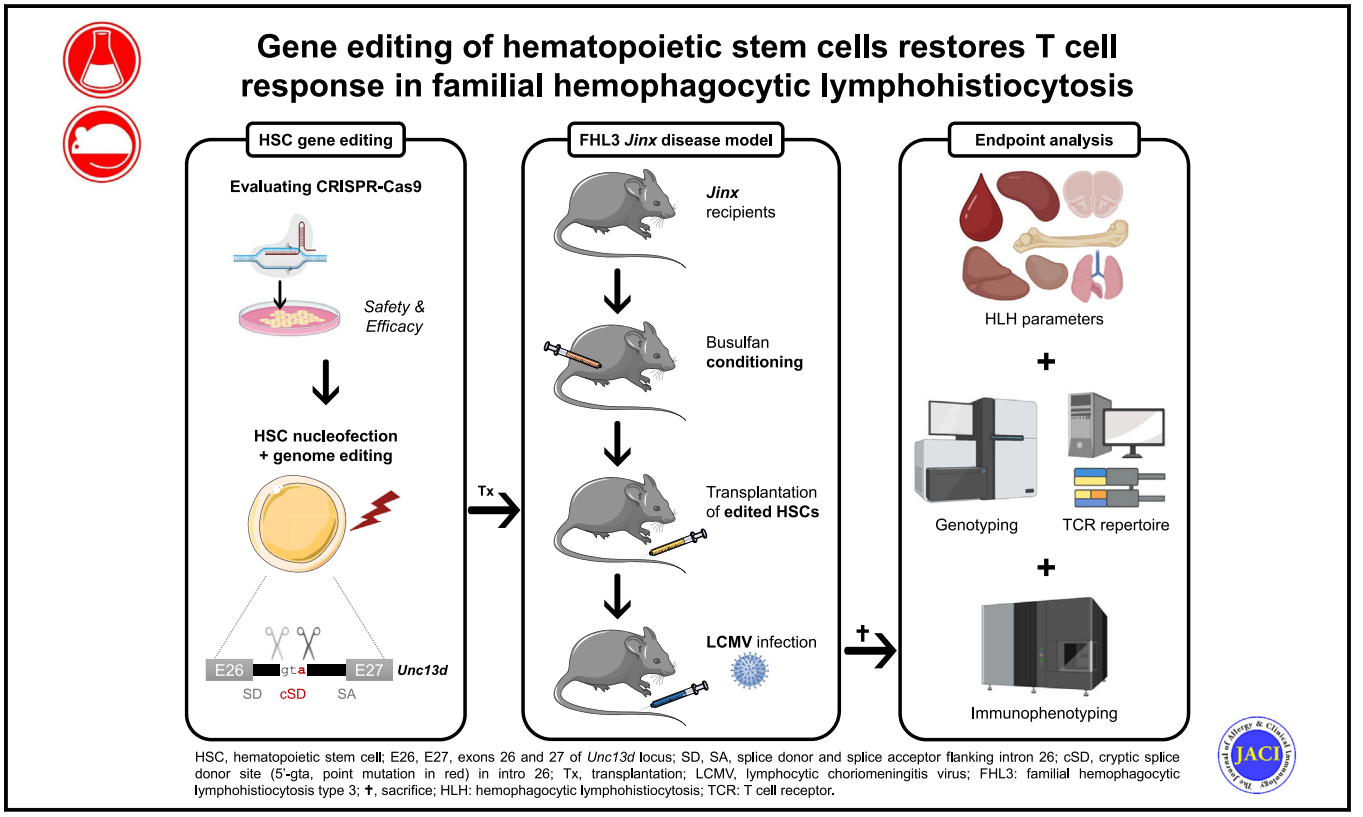

From [a]the Institute for Transfusion Medicine and Gene Therapy, [b]the Center for Chronic Immunodeficiency, [c]the Institute for Immunodeficiency, and [d]the Institute of Neuropathology, Medical Center–University of Freiburg, Freiburg; [e]Ph.D. Program, Faculty of Biology, University of Freiburg, Freiburg; [f]the Department of Internal Medicine I, Medical Center–University of Freiburg, Freiburg; [g]German Cancer Consortium, Partner Site Freiburg & German Cancer Research Center, Heidelberg; [h]Spemann Graduate School of Biology and Medicine, University of Freiburg, Freiburg; [i]the Institute of Medical Bioinformatics and Systems Medicine, Medical Center–University of Freiburg, Freiburg; [j]Faculty of Medicine, University of Freiburg, Freiburg; and [k]the Institute of Surgical Pathology, Medical Center–University of Freiburg, Freiburg.

*These authors contributed equally to this work.

‡These authors contributed equally to this work.

§Anna L. Illert, MD, is currently at the Department of Internal Medicine III, Klinikum recht der Isar, Technical University Munich, Munich, Germany.

Received for publication May 7, 2023; revised July 4, 2023; accepted for publication August 8, 2023.

Available online August 16, 2023.

Corresponding author: Toni Cathomen, PhD, Institute for Transfusion Medicine and Gene Therapy, Medical Center–University of Freiburg, Hugstetter Strasse 55, 79106 Freiburg, Germany. E-mail: toni.cathomen@uniklinik-freiburg.de.

0091-6749

https://doi.org/10.1016/j.jaci.2023.08.003

Background: Hemophagocytic lymphohistiocytosis (HLH) is a hyperinflammatory disorder characterized by a life-threatening cytokine storm and immunopathology. Familial HLH type 3 (FHL3) accounts for approximately 30% of all inborn HLH cases worldwide. It is caused by mutations in the *UNC13D* gene that result in impaired degranulation of cytotoxic vesicles and hence compromised T-cell- and natural killer-cell-mediated killing. Current treatment protocols, including allogeneic hematopoietic stem cell (HSC) transplantation, still show high mortality.

Objective: We sought to develop and evaluate a curative genome editing strategy in the preclinical FHL3 *Jinx* mouse model. *Jinx* mice harbor a cryptic splice donor site in *Unc13d* intron 26 and develop clinical symptoms of human FHL3 upon infection with lymphocytic choriomeningitis virus (LCMV).

Methods: We employed clustered regularly interspaced short palindromic repeats (CRISPR)-Cas technology to delete the disease-causing mutation in HSCs and transplanted *Unc13d*-edited stem cells into busulfan-conditioned *Jinx* recipient mice. Safety studies included extensive genotyping and chromosomal aberrations analysis by single targeted linker-mediated PCR sequencing (CAST-Seq)-based off-target analyses. Cure from HLH predisposition was assessed by LCMV infection.

Results: Hematopoietic cells isolated from transplanted mice revealed efficient gene editing (>95%), polyclonality of the T-cell receptor repertoire, and neither signs of off-target effects nor leukemogenesis. *Unc13d* transcription levels of edited and wild-type cells were comparable. While LCMV challenge resulted in acute HLH in *Jinx* mice transplanted with mock-edited HSCs, *Jinx* mice grafted with *Unc13d*-edited cells showed rapid virus clearance and protection from HLH.

Conclusions: Our study demonstrates that transplantation of CRISPR-Cas edited HSCs supports the development of a functional polyclonal T-cell response in the absence of genotoxicity-associated clonal outgrowth. (J Allergy Clin Immunol 2024;153:243-55.)

Key words: *Autologous stem cell transplantation, CAST-Seq, CRISPR-Cas, gene therapy, genome editing, genotoxicity, hemophagocytic lymphohistiocytosis, hyperinflammation, T-cell repertoire*

Abbreviations used

BM:	Bone marrow
CAST-Seq:	Chromosomal aberrations analysis by single targeted linker-mediated PCR sequencing
CRISPR:	Clustered regularly interspaced short palindromic repeats
FHL:	Familial hemophagocytic lymphohistiocytosis
HLH:	Hemophagocytic lymphohistiocytosis
HSC:	Hematopoietic stem cell
LCMV:	Lymphocytic choriomeningitis virus
NGS:	Next-generation sequencing
PB:	Peripheral blood
PFU:	Plaque-forming unit
RNP:	Ribonucleoprotein
TCR:	T-cell receptor
wt:	Wild-type

Hemophagocytic lymphohistiocytosis (HLH) is a life-threatening, systemic hyperinflammatory disorder. Familial hemophagocytic lymphohistiocytosis (FHL) comprises a group of rare autosomal-recessive diseases caused by loss-of-function mutations in genes encoding key proteins involved in the cytolytic vesicle-mediated killing by natural killer and T cells.[1-4] The inability of these cytotoxic lymphocytes to efficiently lyse target cells, including antigen-presenting cells, leads to their continuous stimulation, hyperactivation, and massive IFN-γ secretion. This in turn activates macrophages, which further fuels the cytokine storm and leads to tissue infiltration and severe immunopathology. Patients with HLH present with fever, hepatosplenomegaly, cytopenia, and characteristic laboratory features, often accompanied by neurological manifestations.[5,6] Patients with FHL usually develop acute HLH during the first year of life.[7]

Treatment of HLH has 2 phases: 1) control of hyperinflammation and 2) replacement of the defective immune system. For the first phase, standard of care is etoposide-based chemotherapy (HLH-94 treatment protocol). Immunotherapy with anti-thymocyte globulin[8-11] has been used as an alternative first-line therapy, but more promising results have been achieved with the monoclonal anti-CD52 antibody alemtuzumab.[12-15] With these regimens, survival rate of patients with FHL before hematopoietic stem cell (HSC) transplantation ranges from 80% to 95%.[5,8,13] The second phase of treatment is typically achieved by HSC transplantation after myeloablative/reductive conditioning. In the HLH-2004 study, 5-year overall survival of FHL patients with HSC transplantation was 71%, leading to an overall survival of only 59%. More recently, post-transplant survival of up to 100% has been reported with reduced intensity conditioning.[16,17] Due to this and other improvements in patient management, overall survival of FHL patients reached 83% in the period 2016-2021 (Boehm et al, unpublished data, 2023). Nevertheless, limited availability of matched donors, conditioning-related toxicities, and graft-versus-host disease remain important challenges during phase 2 treatment, calling for novel treatment approaches, such as autologous HSC gene therapy.

FHL type 3 (FHL3) is the second most frequent primary HLH and therefore an attractive target for gene therapy. It is caused by biallelic mutations in the *UNC13D* gene that impair the function of MUNC13-4, a protein essential for the degranulation of cytotoxic lymphocytes. *Jinx* mice are used as a preclinical mouse disease model for FHL3. These mice harbor a single C→A transition in the 5′-end of intron 26 of *Unc13d*.[18] This mutation creates a cryptic splice site that causes the incorporation of 53 nucleotides of intronic sequence into the mRNA after exon 26, resulting in translation of 20 aberrant residues followed by a premature stop codon. The produced truncated MUNC13-4 protein is not functional, which abrogates degranulation of cytotoxic lymphocytes. Infection of *Jinx* mice with lymphocytic choriomeningitis virus (LCMV) induces all clinical manifestations used for diagnosis of HLH in patients.[18-21] It was shown previously that lentiviral *UNC13D* gene transfer into *Jinx* HSCs reestablished T-cell function in transplanted *Jinx* mice.[22,23] Furthermore, introduction of an *UNC13D*-encoding lentiviral or retroviral expression cassette restored degranulation capacity in FHL3 patient-derived T cells.[24,25] However, despite the progress in lentiviral gene therapy, concerns about insertional mutagenesis[26-28] and regulation of *UNC13D* expression remain.[29-32]

Targeted genome editing could offer a solution to these problems, but thus far no attempts of establishing gene editing for treatment of primary HLH have been described. Here, we applied a clustered

regularly interspaced short palindromic repeats (CRISPR)/Cas9-based approach to delete the intronic cryptic splice donor site in *Unc13d* with high efficiency. *Jinx* mice transplanted with *Unc13d*-edited HSCs achieved high chimerism without detectable off-target effects. Importantly, these mice were fully protected from LCMV-induced HLH and showed neither signs of clonal T-cell expansion nor leukemogenesis. This study provides important preclinical evidence of efficacy and safety of HSC gene editing to treat FHL.

METHODS

Mouse strains

Mouse experiments were approved by the competent authority (G-21/023, Regierungspräsidium Freiburg). *Jinx* (C57BL/6J-Unc13dJinx/Mmucd) and wild-type (wt) mice (C57BL/6N) were bred as previously described.[21] P14-TCR transgenic mice [B6.D2-Tg(TcrLCMV)318Sdz/JDvsJ] were provided by Prof. Hanspeter Pircher (Freiburg, Germany)[33] and crossed with *Jinx* mice to generate a P14.*Jinx* line.

Nucleofection

Ribonucleoproteins (RNPs) were preassembled at a 1:3 molar ratio by incubating 18.3 pmol (3 μg) of Cas9 protein (IDT, Coralville, Iowa) with 55 pmol of gRNA (Biolegio, Nijmegen, The Netherlands) (Table E1 in this article's Online Repository at www.jacionline.org) for 10 minutes at room temperature. Nucleofections were performed with RNPs or 1 μg of PureBoost EGFP-mRNA (Cellerna, Baesweiler, Germany) using a 4D-Nucleofector (Lonza, Basel, Switzerland).

Functional T-cell assays

For *in vivo* evaluation, $CD8^+$ T cells were purified from splenocytes (StemCell Technologies, 19853, Vancouver, Canada), activated for 3 days with beads coated with CD3ε and CD28 antibodies (Miltenyi Biotec, 130-093-627, Bergisch Gladbach, Germany) in RPMI 1640 medium (Gibco, Life Technologies, Waltham, Mass) supplemented with 10% FCS (PAA, BioPath Stores, Cambridge, UK), Pen/Strep (Sigma-Aldrich, St Louis, Mo), and murine IL-2 (10 U/mL) (Peprotech, Hamburg, Germany) before nucleofection (P4-CM137).[34] After 24 hours, 10^5 *Unc13d*-edited $CD8^+$ T cells were infused in recipients via tail vein injection. Mice were infected 8 hours later with 200 PFU of LCMV-WE[35] (provided by Dr. Lehmann-Grube, Hamburg, Germany) and euthanized after 7 days. *In vitro* degranulation assay was performed 7 days after initial T-cell activation (as above) or with splenocytes from LCMV-challenged chimeras. Cells were stimulated for 4 hours at 37°C in supplemented RPMI 1640 medium containing anti-CD107a-PE (Table E2 in the Online Repository at www.jacionline.org) with either plate-bound anti-murine CD3 antibody (10 μg/mL) (BD Bioscience, clone 17A2, Franklin Lakes, NJ) for $CD8^+$ T cells or LCMV-GP_{33-41} peptide (1 μM) (PolyPeptide, Strasbourg, France) using splenocytes. Killing capacity of T cells was determined on LCMV-GP_{33-41} pulsed EL-4 target cells in a chromium-51-release assay.[36]

Transplantation of gene-edited HSCs and LCMV challenge

Lineage-negative HSCs (Miltenyi Biotec, 130-090-858. Bergisch Gladbach, Germany) from femur and tibia-derived bone marrow (BM) were stimulated for 3 hours in StemSpan SFEM II medium (StemCell Technologies, Vancouver, Canada) supplemented with L-glutamine (20 mM) (Gibco, Life Technologies), mSCF, mTPO, and hIGF2 (20 ng/mL each) plus hIGF2 and mIL-3 (10 ng/mL each) (Peprotech. Hamburg, Germany) before nucleofection (P4-CA137). After 20 hours of culture without mIL-3, 10^6 cells were infused via tail vein to recipients conditioned with 5 cycles of busulfan (20 mg/kg)[37] (Fresenius Kabi, Bad Homburg, Germany) over 5 consecutive days. From week 6, tail bleeding of mice was done biweekly to monitor chimerism, editing frequency, and potential leukemogenesis. Following 14 to 34 weeks of reconstitution, mice were infected via intravenous injection with 200 PFU of LCMV-WE and euthanized after 12 to 15 days.

Flow cytometry

All stainings with conjugated antibodies (Tables E2 and E3 in the Online Repository at www.jacionline.org) were performed for ≥20 minutes at 4°C in the dark after removal of red blood cells (eBioscience, 00-4333-57, San Diego, Calif) and exclusion of dead cells from spectral flow cytometry samples[38] (Thermo Fisher Scientific, L34959. Waltham, Mass). Sample acquisition was conducted on a BD LSR Fortessa (BD, San Jose, Calif) device or on Sony SP6800 and ID7000 spectral analyzers (Sony Biotechnology, San Jose, Calif), and data were analyzed with FlowJo (versions 9/10, BD Biosciences, San Jose, Calif).

Histology and blood and serum analyses

Histology and blood and serum analyses were performed as previously described.[21,36] IFN-γ was detected using LEGENDplex Mouse Inflammation Panel (Biolegend, 740446, San Diego, Calif). Blood counts were determined using the scil Vet abc hematology analyzer. Pappenheim staining of blood smears was done,[39] and representative images were acquired with Zeiss AxioImager M2m (Zeiss AG, Jena, Germany).

Genotyping and Off-Target Analysis

PCR amplification (NEB, M0493L, Ipswich, Mass) from genomic DNA (Macherey-Nagel, 740952, Dueren, Germany) was performed on the *Jinx* intron 26 region, followed by T7E1 analysis (NEB, M0302L) or targeted amplicon next-generation sequencing (NGS) (Genewiz, Burlington, Vt) (Table E4 in the Online Repository at www.jacionline.org). Chromosomal aberrations analysis by single targeted linker-mediated PCR sequencing (CAST-Seq) analyses (Table E5 in the Online Repository at www.jacionline.org) were performed on RNP-treated HSCs as described before.[40]

Reverse transcription of total spleen RNA was performed.[41] Then, the cDNA (6 ng) was subjected to digital droplet PCR[25] (Table E6 in the Online Repository at www.jacionline.org) with *Jinx* transcript-specific primers followed by quantification using QuantaSoft (Bio-Rad. Hercules, Calif).

T-cell receptor (TCR) repertoire analysis was adapted from Ko et al.[42] Total RNA was extracted from 10^7 splenocytes or $CD8^+$ T

cells (Qiagen, 74106, Venlo, The Netherlands), reverse transcribed (500 ng), and treated with uracil-DNA glycosylase (NEB). TCR sequences were amplified in PCRI (2 μL cDNA) and PCRII (3 μL PCRI) using Primers and SmartN oligos (IDT) (Table E7 in the Online Repository at www.jacionline.org). After agarose gel separation, 400- to 800-bp-long PCRII fragments were barcoded with Illumina NEBNext Multiplex Oligos in PCRIII (NEB, E7645L). Sequences were processed with Molecular Identifier Groups-Based Error Correction,[43] which included demultiplexing, unique molecular identifier clustering, filtering, V(D)J junction and CDR3 region extraction, and clonotype assembly. Clonotype diversity and visualization was performed in R (immunarch package),[44] and clonotype percentages were grouped into bins ranging from minimal (<0.0001) to hyperexpanded (>0.01).

Statistical analysis

One-way analysis of variance comparing multiple samples followed by unpaired *t* test and Mann-Whitney *U* test were conducted using GraphPad Prism 9.

Data sharing

High-throughput data are available at Gene Expression Omnibus under accession numbers GSE225269 (CAST-Seq), GSE225534 (TCR repertoire analysis), and GSE225540 (targeted amplicon NGS). For other data, contact the corresponding author (toni.cathomen@uniklinik-freiburg.de).

RESULTS

Identifying the lead candidate for efficient and safe modification of the intronic mutation

Six CRISPR-Cas9 gRNAs were designed to target the C→A transition in *Unc13d* intron 26 either upstream (u1-u3) or downstream (d4-d6) (Fig E1, *A*, in the Online Repository at www.jacionline.org). They were tested separately and in 9 possible upstream/downstream combinations in a *Jinx* reporter cell line harboring a green fluorescent protein gene interjected by *Jinx* intron 26 to evaluate their potential to disrupt the cryptic splice donor site (Fig E1, *B*). Flow cytometry and T7E1 analysis revealed efficient editing with upstream/downstream combinations, yielding up to approximately 80% GFP^+ cells and approximately 100% of modified alleles, respectively (Fig E1, *C* and *D*). To evaluate this double-hit strategy, ie, an upstream/downstream combination to excise the cryptic splice donor site (Fig 1, *A*) in primary cells, we performed nucleofections of *Jinx* T cells with the best CRISPR-Cas combinations u1/d4, u1/d6, u3/d4, and u3/d6 and analyzed Munc13-4 restoration in a degranulation assay based on CD107a surface expression. Gene editing of *Jinx* T cells with combinations u1/d4 and u3/d4 resulted in 72% ± 5% $CD8^+/CD107a^+$ cells, which was comparable to the fraction of $CD8^+/CD107a^+$ wt cells (73% ± 9%) (Fig 1, *B*). NGS confirmed high editing frequencies with combinations u1/d4 (83%) and u3/d4 (82%) compared with u1/d6 (58%) and u3/d6 (56%) (Fig 1, *C*). Some double-hit approaches yielded a large fraction of perfect excision events, eg, 31% for u3/d4 and 20% for u1/d4 (Fig 1, *C*). Next, we assessed the off-target effects associated with the expression of the 2 best performing CRISPR-Cas combinations, u1/d4 and u3/d4, in *Jinx* HSCs by employing CAST-Seq.[44] While on-target aberrations were confirmed for both combinations (Fig 1, *D*), the combination u1/d4 prompted chromosomal translocations between the *Unc13d* on-target and 6 off-target sites, with chromosomes X and 7 being the most frequent translocation partners (Fig 1, *D* and *E*). By contrast, transfer of u3/d4 RNPs did not lead to off-target effects and was therefore considered the most efficient and most specific combination to move forward. Henceforth CRISPR-Cas combination u3/d4 is simply referred to as RNP.

Genome editing restores functionality of *Jinx* $CD8^+$ T cells *in vivo*

Activity and persistent functional rescue of *Unc13d*-edited T cells were evaluated in a short-term adoptive transfer *in vivo* model employing $CD45.1^+$ P14 mice-derived T cells, which express a transgenic TCR that recognizes the GP_{33-41} LCMV epitope.[33] This yields a rapid, highly reactive monoclonal immune response upon LCMV challenge. $CD8^+$ T cells were isolated either from P14 mice crossed with *Jinx* (P14.*Jinx*) or from P14.wt mice as a control. Upon nucleofection with RNPs (u3/d4), the edited T cells were infused into $CD45.2^+$ wt recipient mice. At 7 days after infection with LCMV (Fig 2, *A*), the T-cell chimerism determined by CD45.1 (donor) and CD45.2 (recipient) expression in spleen was comparable between all 3 groups, with 75% ± 2% of $CD8^+$ T cells derived from the respective P14 grafts (Fig 2, *B*). Next, an *in vitro* degranulation assay with the *in vivo* challenged T cells was performed. The degranulation capacity (estimated by CD107a surface expression) of edited P14.*Jinx* T cells (76% ± 5% $CD8^+/CD107a^+$ cells) was similar to the control (P14.wt) and significantly higher than the degranulation frequency (24% ± 2%) of T cells isolated from mice infused with nonedited P14.*Jinx* T cells (Fig 2, *C*). Then, genotyping by T7E1 assay and quantification of misspliced *Unc13d* transcripts were performed. We found that 65% ± 7% of *Unc13d* alleles were edited at the genome level (Fig 2, *D*), which correlated well with a significant reduction of incorrectly spliced *Unc13d* transcripts (Fig 2, *E*).

Gene editing of *Jinx* HSCs restores functionality of the immune system

To evaluate whether *Unc13d*-edited *Jinx* HSCs can revoke the FHL3-associated predisposition to HLH, we transplanted busulfan-preconditioned *Jinx* mice or wt recipients with mock-edited wt HSCs (wt→wt), HSCs from mock-edited *Jinx* mice (J→J), or HSCs of *Unc13d*-edited *Jinx* mice (J^{RNP}→J) (Fig 3, *A*). Results obtained from mid-term (14-16 weeks) and long-term (24-34 weeks) reconstitution experiments showed no substantial differences and were therefore combined. Assessment of the chimerism revealed >95% of $CD45.1^+$ donor-derived cells in the BM, spleen, and blood, independently of the group and comparable chimerism in all sublineages (Fig E2, *A-D*, in the Online Repository at www.jacionline.org). J→J mice contained a higher fraction of $CD11b^+$ cells (neutrophils/monocytes/macrophages) but lower percentages of lymphocytes (CD8/CD19) when compared with wt→wt and J^{RNP}→J mice (Fig E2, *E*).

After full reconstitution (14-34 weeks post-transplantation), chimeric mice were infected with LCMV and body weight was monitored over a 2-week period (Fig 3, *B*). A significant weight loss between days 6 and 10 after infection was apparent in J→J

mice, whereas $J^{RNP} \rightarrow J$ chimeras were able to maintain their body weight in a similar fashion as wt → wt mice. End point analysis on day 15 after infection showed a significantly lower ear temperature in J → J mice compared with $J^{RNP} \rightarrow J$ and wt → wt chimeras (Fig 3, *C*), indicating centralization of circulation that corresponds to fever in patients with HLH. Further analyses revealed pronounced hepatosplenomegaly, strong infiltrations of lymphocytes, and massive tissue destruction in J → J mice, which was not evident in either $J^{RNP} \rightarrow J$ or wt → wt chimeras (Fig 3*D* and *E*; Fig E3, *A*, in the Online Repository at www.jacionline.org). Furthermore, J → J mice showed a significant reduction in white blood cells, hemoglobin, and platelets (Fig 3, *F-H*). While a difference in triglyceride levels was not apparent (Fig E3, *B*, in the Online Repository at www.jacionline.org), serum analyses revealed significantly increased ferritin as well as elevated glutamate-pyruvate transaminase, lactate dehydrogenase, sCD25, and IFN-γ levels in J → J mice (Fig 3, *I-M*). Moreover, viral titer analysis showed LCMV persistence in J → J mice, while wt → wt and $J^{RNP} \rightarrow J$ mice cleared the virus from spleen, liver, lung, kidney, and brain (Fig. 3, *N*). In sum, *Jinx* mice transplanted with nonedited *Jinx* HSCs (J → J) displayed the full clinical picture of an active HLH on LCMV infection, while *Jinx* mice grafted with *Unc13d*-edited *Jinx* HSCs ($J^{RNP} \rightarrow J$) recovered similarly well as wt → wt chimeras.

As defective cytotoxicity causes antigen persistence, and as a consequence continuous stimulation of the disease-inducing T cells, we were interested in characterizing the phenotype of graft-derived $CD8^+$ T cells *ex vivo*. Flow cytometric analysis revealed a high percentage of $CD8^+$ T cells expressing inhibitory receptors (PD-1, Lag-3, and Tim3) and Tox in J → J mice. In contrast, $CD8^+$ T cells in recipients of *Unc13d*-edited *Jinx* HSCs ($J^{RNP} \rightarrow J$) had downregulated inhibitory receptors and Tox comparable to wt → wt chimeras (Fig 4, *A-C*). In line with this finding, we observed that impaired degranulation capacity of LCMV-GP_{33-41} peptide stimulated $CD8^+$ T cells isolated from J → J mice, while $CD8^+$ T cells derived from $J^{RNP} \rightarrow J$ mice degranulated as effectively as T cells from wt → wt mice (Fig 4, *D*). Correspondingly, graft-derived splenocytes isolated from $J^{RNP} \rightarrow J$ and wt → wt mice exhibited high cytolysis on LCMV-GP_{33-41} pulsed target cells, whereas J → J chimera-derived T cells were not able to sufficiently kill the target cells (Fig 4, *E*). In accordance with these findings, mRNA analysis showed a significantly reduced number of misspliced *Jinx* transcripts in J^{RNP} graft-derived $CD8^+$ T cells compared with J → J mice-derived cells (Fig 4, *F*). In sum, similar $CD8^+$ T-cell differentiation and function were observed in $J^{RNP} \rightarrow J$ and wt → wt mice, underlining the functional potency of $CD8^+$ T cells originating from *Unc13d*-edited HSCs.

Therapy-associated genotoxicity

Similar to a genome editing clinical trial in humans, our protocol combined chemotherapy with gene editing in HSCs. For that reason, particular attention was paid to the risk of therapy-associated genotoxicity, such as clonal expansion and potential leukemogenesis. We first analyzed genomic DNA of edited HSCs before transplantation (*in vitro*) or of cells isolated from *Jinx* mice engrafted with *Unc13d*-edited *Jinx* HSCs ($J^{RNP} \rightarrow J$), including DNA from peripheral blood (PB) or BM after LCMV infection. Editing frequencies ranged from 68% ± 8% (HSCs) to 85% ± 9% (BM) without a significant difference between samples originating from different sources (Fig 5, *A*). A detailed analysis of the top 10 editing outcomes in each sample revealed 32 different indels that were heterogeneous in both distribution and frequency (Fig 5, *B*). The most prominent deletion in 12 of 13 samples, with frequencies of 53% ± 16%, was a perfect 24-bp excision derived from the double-hit event.

Given that clonal cell expansion is a hallmark of leukemogenesis, we monitored genotypic changes over time by assessing the fate of an edited HSC sample ($J^{RNP} \rightarrow J$ mouse grafted with HSC sample Z: J^{RNP} Z) (Fig 5, *B*). We determined the top 1000 indels in HSC, PB, and BM samples of 3 mice (1^z-3^z) based on their frequency. We found on comparison that only approximately 12% of indel outcomes were shared among the 3 compartments (Fig 5, *C*). Greater than 80% of indel events were uniquely present in the HSC compartment, and about 45% were detected only in either PB- or BM-derived cells. The overlap between PB and BM samples was in the range of approximately 40%. In conclusion, these results revealed an enormous heterogeneity of editing outcomes and indicate that indel distribution analysis can serve as a simple means to assess clonal expansion.

As immune cell infiltration into the BM is a characteristic trait of acute HLH, we separated the BM of 3 $J^{RNP} \rightarrow J$ mice (mice 8-10) into lineage-negative (engrafted HSCs) and lineage-positive (infiltrating/circulating immune cells) fractions. NGS analysis showed comparable editing frequencies of 85% ± 11% in both fractions (Fig 5, *D*). Heterogeneity between individual mice was confirmed by comparison of the top 10 indel events in each mouse (Fig 5, *E*). Intraindividual analysis of the top 1000 indels revealed about 67% overlap between the lineage-negative/lineage-positive fractions in each mouse, with no evidence for expansion of a single clone but rather a high conservation of genome editing outcomes between engrafted and infiltrating/circulating cells in the same recipient (Fig 5, *F*).

To verify absence of apparent leukemogenesis in the myeloid compartment, immunophenotyping of PB samples of wt → wt and $J^{RNP} \rightarrow J$ mice 30 to 34 weeks post-transplantation was performed. Analysis of PB before LCMV infection revealed comparable white blood cell counts and no detectable blasts in blood smear samples (Fig E4, *A-C*, in the Online Repository at www.jacionline.org). After LCMV infection, the absence of myeloid progenitor cells in the spleen, but not in the BM, of mock-edited *Jinx* mice was uncovered (Fig E5, *A-E*, in the Online Repository at www.jacionline.org), while the fraction of megakaryocyte-erythroid progenitor cells was comparable between all groups and organs (Fig E5, *F*). Because it is conceivable that a potential preleukemic event in T cells leads to clonal transformation after viral infection, we analyzed the TCR repertoire of splenocytes from LCMV-challenged mice. While unchallenged mice (wt^- or P14.wt^-) served as a negative baseline and LCMV-infected wt^+ mice as a comparator, LCMV-infected P14.wt^+ → wt T-cell chimeric mice (Fig 2) were included as a reference for a widely monoclonal T-cell expansion (Fig E6 in the Online Repository at www.jacionline.org). Samples derived from uninfected wt or *Jinx* mice revealed a heterogeneous TCR profile with an even distribution of comparable CD3 lengths (approximately 10-20 residues). By contrast, samples isolated from P14 T-cell bearing mice displayed a highly overrepresented fraction, representing T cells harboring the transgenic TCR. TCR diversity of P14 T cells was low and, as expected, further decreased after LCMV infection (Fig 6, *A*). LCMV infection also led to a reduced diversity score in wt T cells, but the overall TCR diversity was significantly higher than in P14 T cells.

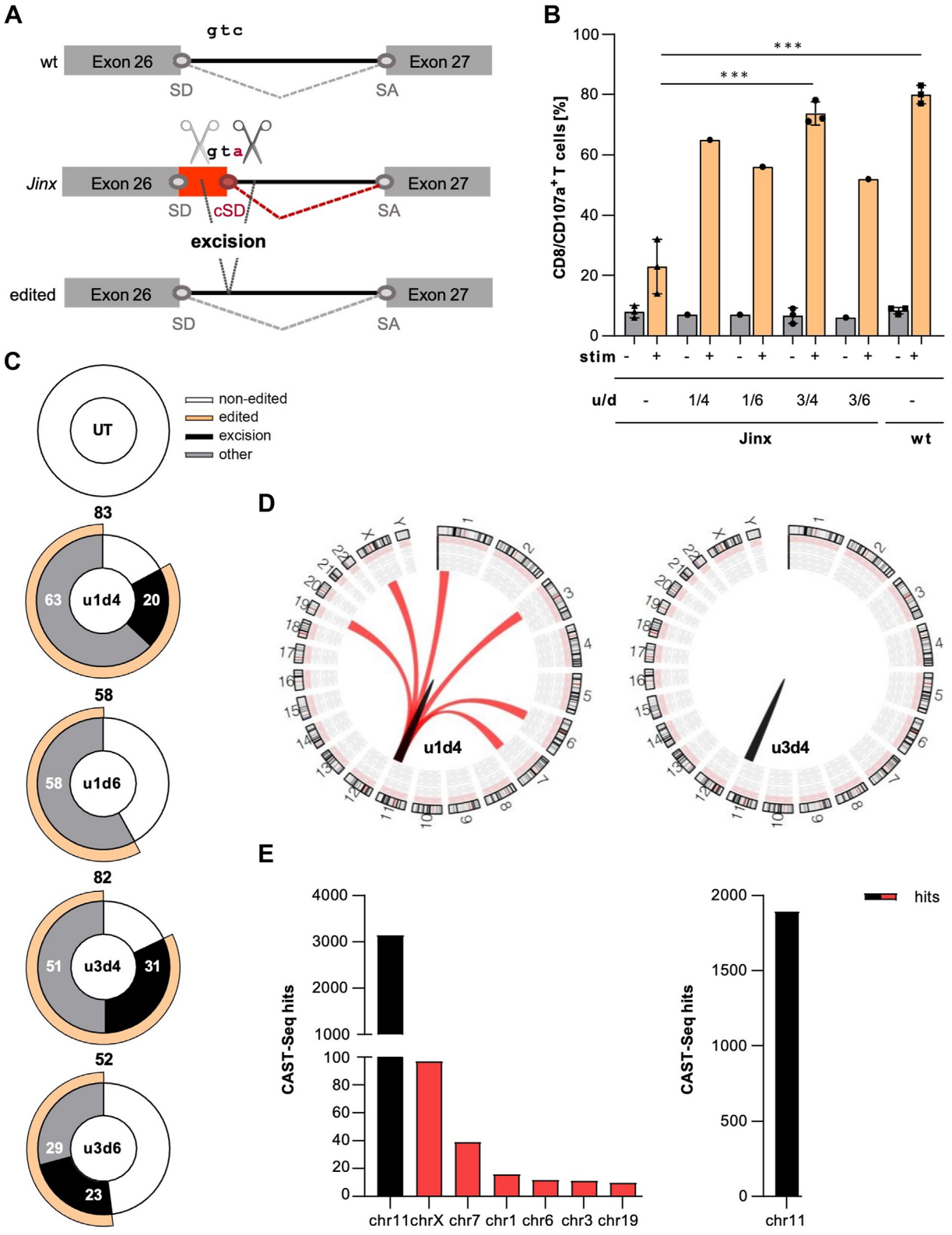

FIG 1. Efficacy and specificity of CRISPR-Cas9 gene editing approach. **(A)** Strategy. Intron 26 splicing in *Jinx* mice is restored by excising the cryptic splice donor site with 2 CRISPR-Cas9 nucleases, one cleaving upstream and the other downstream of the mutation. **(B)** Functional restoration of gene-edited T cells *in vitro*. *Jinx* $CD8^+$ T cells were edited with CRISPR-Cas9 combinations u1/d4, u1/d6, u3/d4, or u3/d6. Degranulation was determined by assessing CD107a surface expression after stimulation with anti-CD3 antibody *(orange bars)* vis-à-vis to unstimulated controls *(gray bars)*. Mean values ± SD are depicted

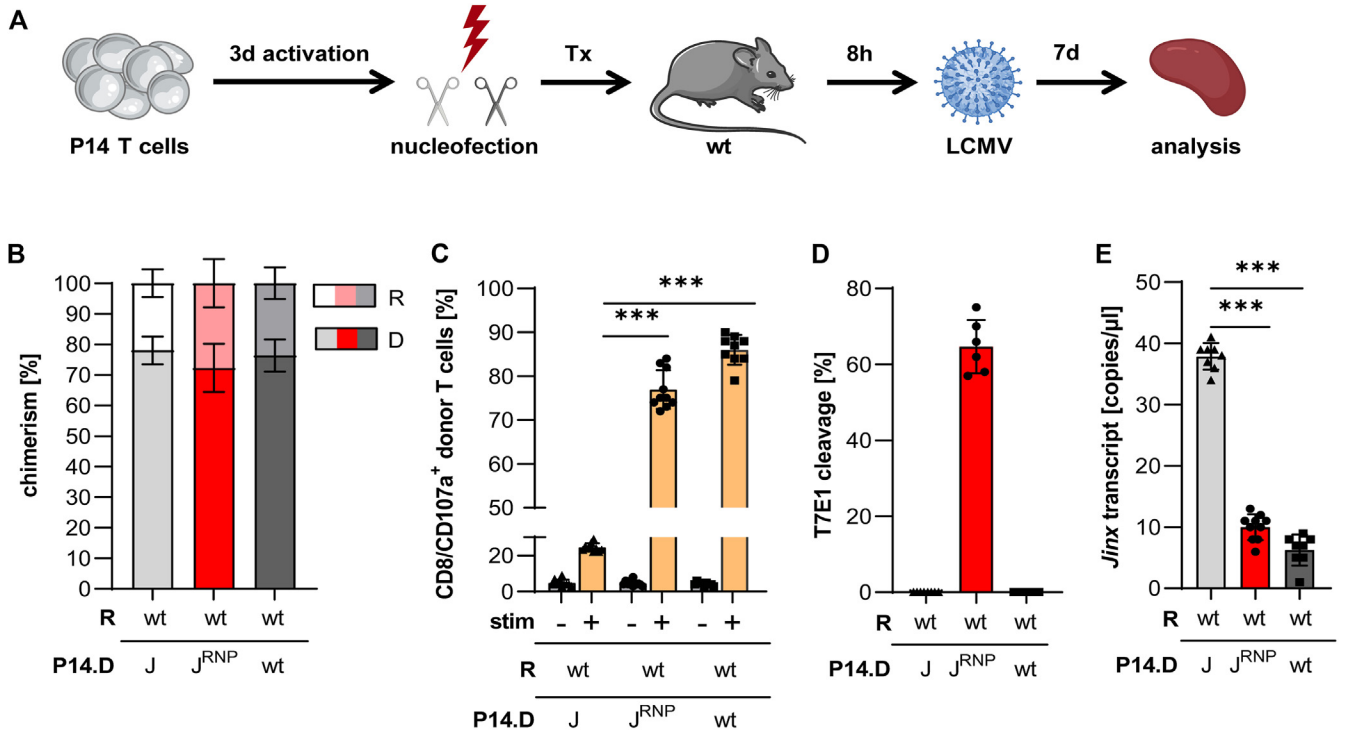

FIG 2. Functional restoration of *Unc13d*-edited P14.*Jinx* CD8$^+$ T cells. **(A)** Workflow. The wt recipient mice were infused with *Unc13d*-edited P14.*Jinx* donor CD8$^+$ T cells *(red bars)*, followed by infection with LCMV and end point analysis. P14.wt *(dark gray bars)* and nonedited P14.*Jinx (light gray bars)* donor T cells served as controls. **(B)** T-cell chimerism. CD8$^+$ T-cell chimerism was determined based on the fraction of CD45.1$^+$ (donor) vs CD45.2$^+$ (recipient) cells (n = 8-10 from 3 independent experiments with 3-4 different donors). **(C)** T-cell function. Degranulation capacity of P14.*Jinx* CD8$^+$ T cells was assessed by evaluating CD107a-surface expression after stimulation *(+, orange bars)* with anti-CD3 antibody vis-à-vis unstimulated controls *(−, gray bars)*. **(D)** Gene editing frequency. Fraction of edited *Unc13d* alleles was determined by T7E1 assay (n = 6, 2 separate samples from 3 donors). **(E)** Concentration of misspliced *Unc13d* transcripts. The number of incorrectly spliced *Unc13d* mRNAs, as determined by ddPCR, is indicated as mean ± SD. Unpaired *t* test: ***$P \leq .001$. *D,* Donor; *J, Jinx*; *P14.D,* P14.*Jinx* donor; *J^{RNP}, Unc13d*-edited *Jinx* HSCs; *R,* recipient. Figure was in part created with Servier Medical Art (https://smart.servier.com/) or BioRender (https://www.biorender.com/).

Crucially, TCR diversity in mice transplanted with *Unc13d*-edited HSCs was similar to wt mice transplanted with wt HSCs. The complementing assessment of TCR clonality exposed a hyperexpanded monoclonal fraction, comprising 82% ± 1% of T cells, in LCMV-infected P14.wt→wt T-cell chimera, but no significant differences in TCR clonality between the wt→wt and J^{RNP}→J groups (Fig 6, *B*). In summary, our evaluation of mice transplanted with *Unc13d*-edited HSCs substantiated the enormous heterogeneity of genome editing outcomes both interindividually and intraindividually and validated polyclonal reconstitution of the immune system.

DISCUSSION

Curative treatment for FHL relies on HSC transplantation to restore lymphocyte cytotoxicity and immune regulation. Failure to control HLH hyperinflammation, treatment toxicity, and transplant-associated complications including severe infections and graft rejection or graft-versus-host disease limit the success of current treatment approaches, highlighting the need for novel therapeutic strategies. Lentiviral gene transfer has been successfully employed to treat FHL2 and FHL3 in murine disease models and is expected to be evaluated in phase 1/2 gene therapy clinical trials.[22,45,46] The high production costs of viral vector stocks, the residual risk of lentiviral vector-associated insertional mutagenesis,[26-28] and the potential need to regulate *UNC13D* expression[29-32] warrant testing alternative genome engineering strategies. In this study, we evaluated efficacy and safety of gene editing to correct a primary HLH *in vivo*. Our proof-of-concept study aimed to amend a disease-underlying mutation in HSCs and to demonstrate both efficacy and safety in restoring a functional immune system using CRISPR-Cas9 technology. As a proof of

(n = 3 experiments). **(C)** Genotyping. Overall fractions of nonedited *(white)* and edited *Unc13d* alleles *(orange)* are presented, the latter being subdivided into perfect excision *(black)* and various indel events *(gray)*. **(D** and **E)** Assessment of off-target effects in *Jinx* HSCs. Circos plots *(D)* display the qualitative results of CAST-Seq analyses, including on-target aberrations *(black)* and off-target-mediated chromosomal translocations *(red)*. The number of CAST-Seq hits reflect the frequencies of chromosomal translocation events *(E)*. Unpaired *t* test: ***$P \leq .001$. *cSD,* Cryptic splice donor site; *d,* downstream; *SA,* splice acceptor site; *SD,* splice donor site; *u,* upstream; *UT,* untreated cells.

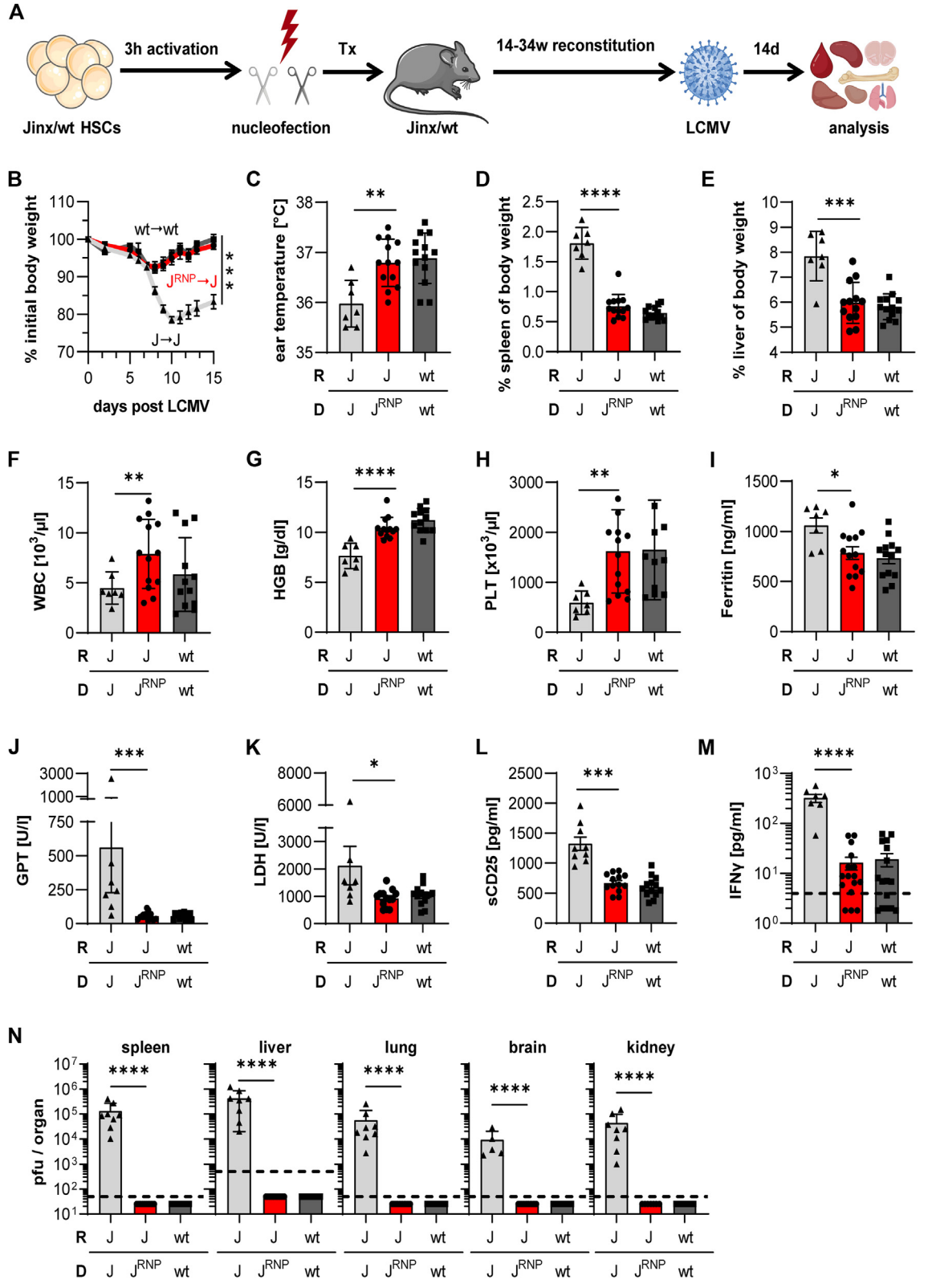

FIG 3. Clinical assessment of *Jinx* mice transplanted with *Unc13d*-edited HSCs. **(A)** Workflow. Preconditioned recipient mice (*Jinx* or wt) were transplanted with donor HSCs (*Jinx*, *Unc13d*-edited *Jinx*, or wt). After 14-34 weeks of reconstitution, mice were infected with LCMV followed by end point analysis. **(B)** Body weight. Relative changes in body weight during infection were monitored. **(C-N)** Clinical end point analysis. Ear temperature *(C)*, weights of spleen *(D)* and liver *(E)* in relation to body weight, white blood cell count *(F)*, hemoglobin concentration *(G)*, platelet count *(H)*, serum concentrations of ferritin *(I)*, glutamate-pyruvate

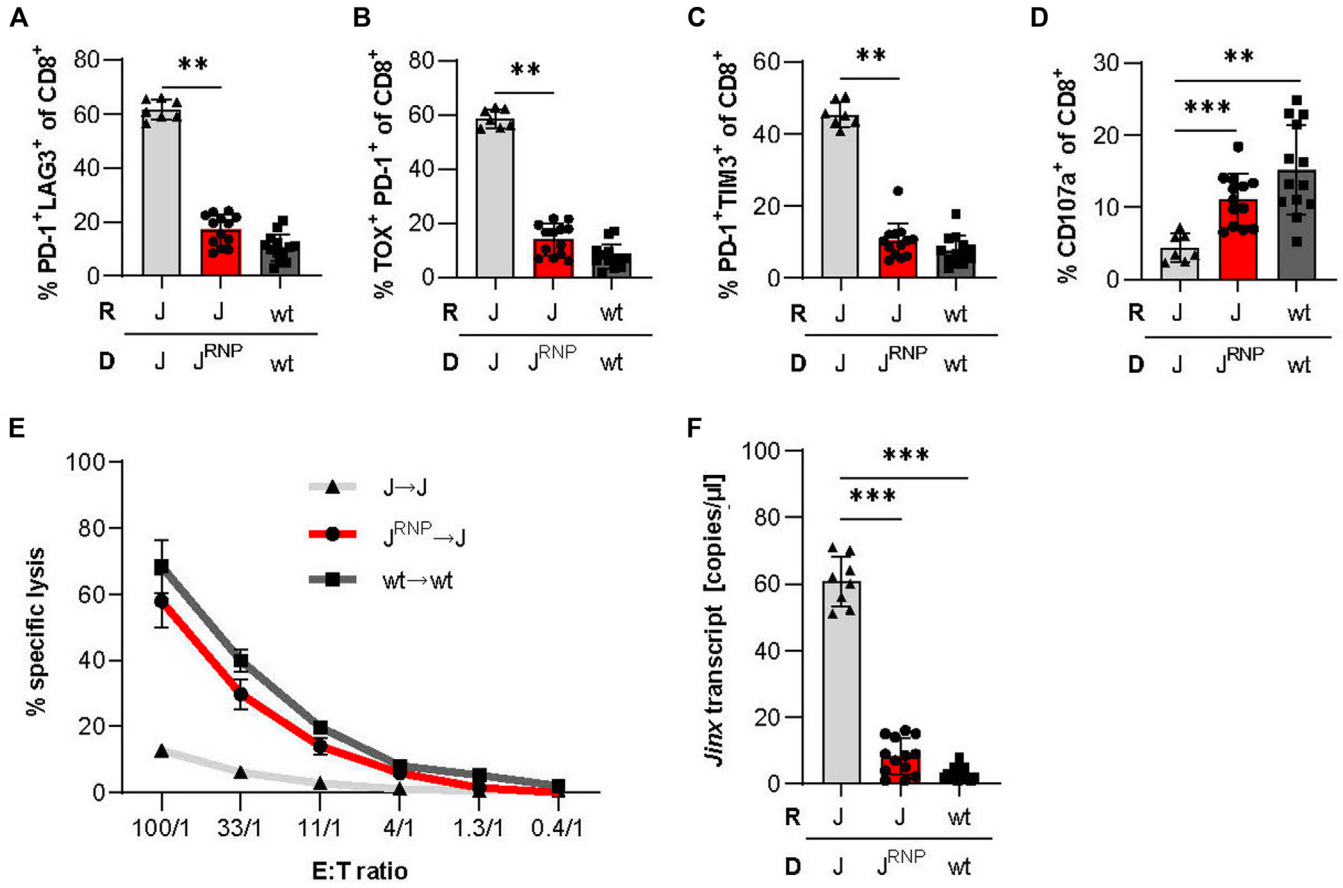

FIG 4. Immunologic assessment of *Jinx* mice transplanted with *Unc13d*-edited HSCs. **(A-C)** T-cell phenotype. Percentages of PD-1$^+$/Lag3$^+$ *(A)*, Tox$^+$PD-1$^+$ *(B)*, and PD-1$^+$Tim3$^+$ *(C)* CD8$^+$ T cells were determined by flow cytometry. **(D)** Antigen-dependent T-cell degranulation. Isolated CD8$^+$ T cells were restimulated with LCMV-GP$_{33-41}$ peptide *in vitro* in the presence of anti-CD107a to determine the degranulation capacity. **(E)** Antigen-specific killing. Splenocytes of LCMV-infected mice were exposed *in vitro* to chromium-51-labeled target cells that have been loaded with LCMV-GP$_{33-41}$ peptide. Chromium-51 release was determined at different effector-to-target ratios. **(F)** Concentration of misspliced *Unc13d* transcripts. The number of incorrectly spliced *Unc13d* mRNAs, as determined by ddPCR, is indicated. *Bars (A-D* and *F)* and *dots (E)* depict mean values ± SD (n = 7-13 mice per group from 2-4 independent experiments with different donors and recipients). Unpaired *t* test *(A-C, E)* and Mann-Whitney *U* test *(D)*: $^{**}P \leq .01$; $^{***}P \leq .001$. *D,* Donor; *E:T,* effector-to-target; *J, Jinx*; *J^{RNP}, Unc13d*-edited *Jinx* HSCs; *R,* recipient.

concept, we chose to edit the cryptic splice site mutation in the *Unc13d* locus of *Jinx* mice. This allowed us to focus on general efficacy and toxicity issues related to genome editing in the stem cell compartment, while leaving the challenges of correcting the variable patient mutations in the *UNC13D* gene to a future study. To align our experiments in the FHL3 mouse model with the clinical situation, our workflow included a conditioning regimen with busulfan, a CRISPR-Cas9-based genome editing approach in HSCs, and a virus infection to trigger HLH. This was followed by a thorough analysis of HLH-defining disease criteria in infected *Jinx* mice and an assessment of potential genotoxicity.

Low-exposure, busulfan-based conditioning is frequently used in the context of autologous HSC gene therapy protocols.[47,48] Yet, its properties as an alkylating agent have also been linked to complications, including secondary solid cancers.[49] Moreover, the combination of busulfan treatment and lentiviral vector-based HSC gene therapy has recently come under scrutiny, as three participants of a sickle cell disease clinical trial (https://classic.clinicaltrials.gov/ct2/show/NCT02140554; ClinicalTrials.gov Identifier NCT02140554) developed acute myeloid leukemia, myelodysplastic syndrome, and anemia, respectively, coupled with trisomy 8.[28,50] Although leukemogenesis was not linked to

transaminase *(J)*, lactate dehydrogenase *(K)*, soluble CD25 *(L)*, IFN-γ *(M)*, and virus titers in indicated organs *(N)* were determined. Mean values ± SD are depicted (n = 7-13 mice from 2-4 independent experiments with different donors and recipients). *Horizontal dashed line (M* and *N)* indicates the detection limit. Unpaired *t* test *(B, C, D, E, H,* and *J)* and Mann-Whitney *U* test *(F, G, I, L, K,* and *M)*: $^{*}P < .05$; $^{**}P \leq .01$; $^{***}P \leq .001$; $^{****}P \leq .0001$. *D,* Donor; *GPT,* glutamate-pyruvate transaminase; *HGB,* hemoglobin; *J, Jinx*; *J^{RNP}, Unc13d*-edited *Jinx* HSCs; *LDH,* lactate dehydrogenase; *PLT,* platelet; *R,* recipient; *sCD25,* soluble CD25; *WBC,* white blood cell. Figure was in part created with Servier Medical Art (https://smart.servier.com/) or BioRender (https://www.biorender.com/).

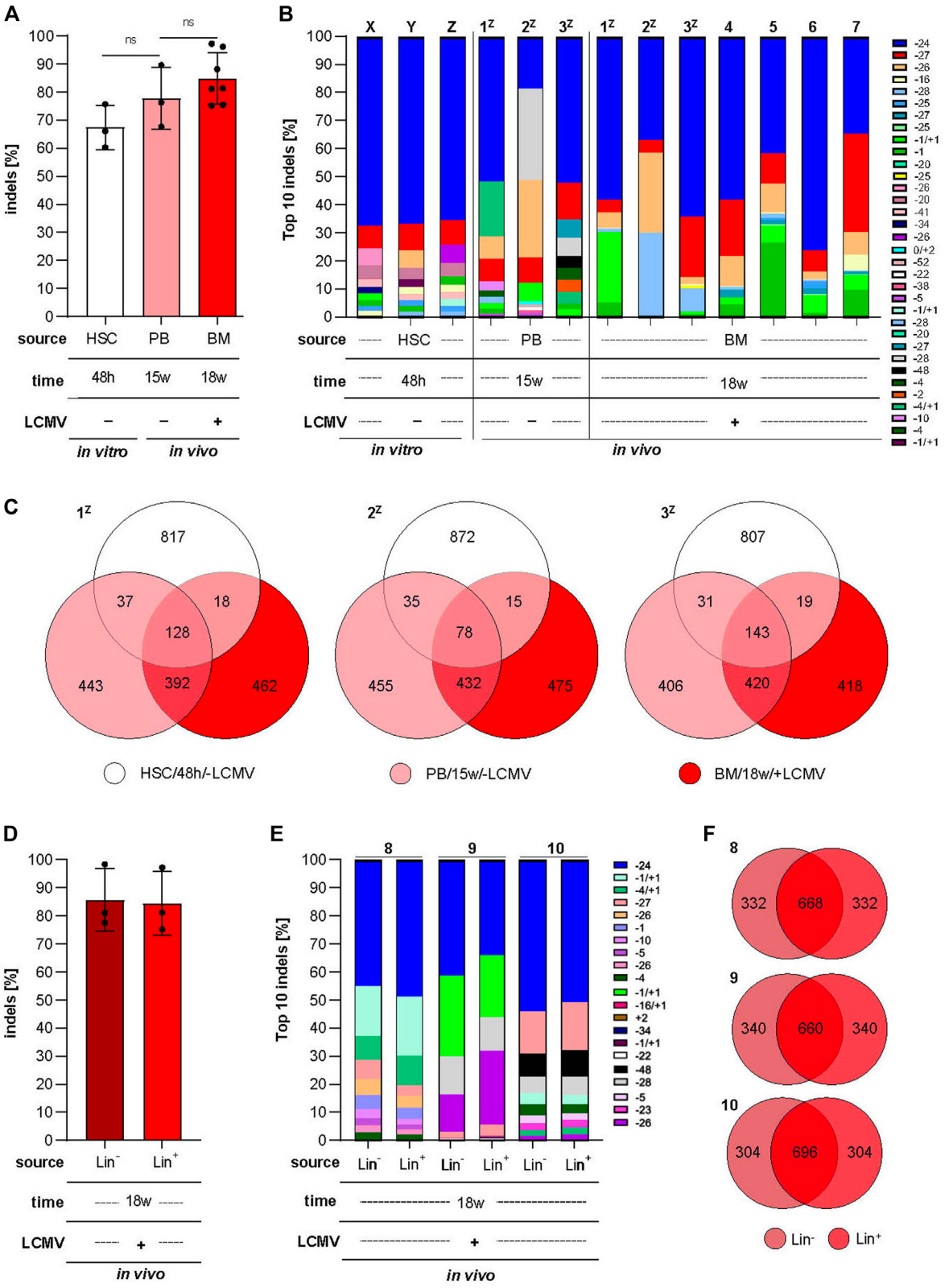

FIG 5. Genotyping. **(A-C)** Interindividual indel distribution. HSCs before transplantation (n = 3 different experiments with 3 different donors: X, Y, Z), PB (n = 3 mice transplanted with the same graft Z: 1^Z-3^Z), or BM (n = 7: 3 mice transplanted with graft Z, 1^Z-3^Z, and 4 mice transplanted with different grafts, 4-7) were subjected to NGS analysis 15 or 18 weeks after engraftment before (PB) and after (BM) LCMV infection. Shown are the fraction of edited *Unc13d* alleles *(A)*, the top 10 indel distributions within a cell fraction *(B)*, and Venn diagrams indicating the distribution of the top 1000 indel events among the cell fractions within a recipient

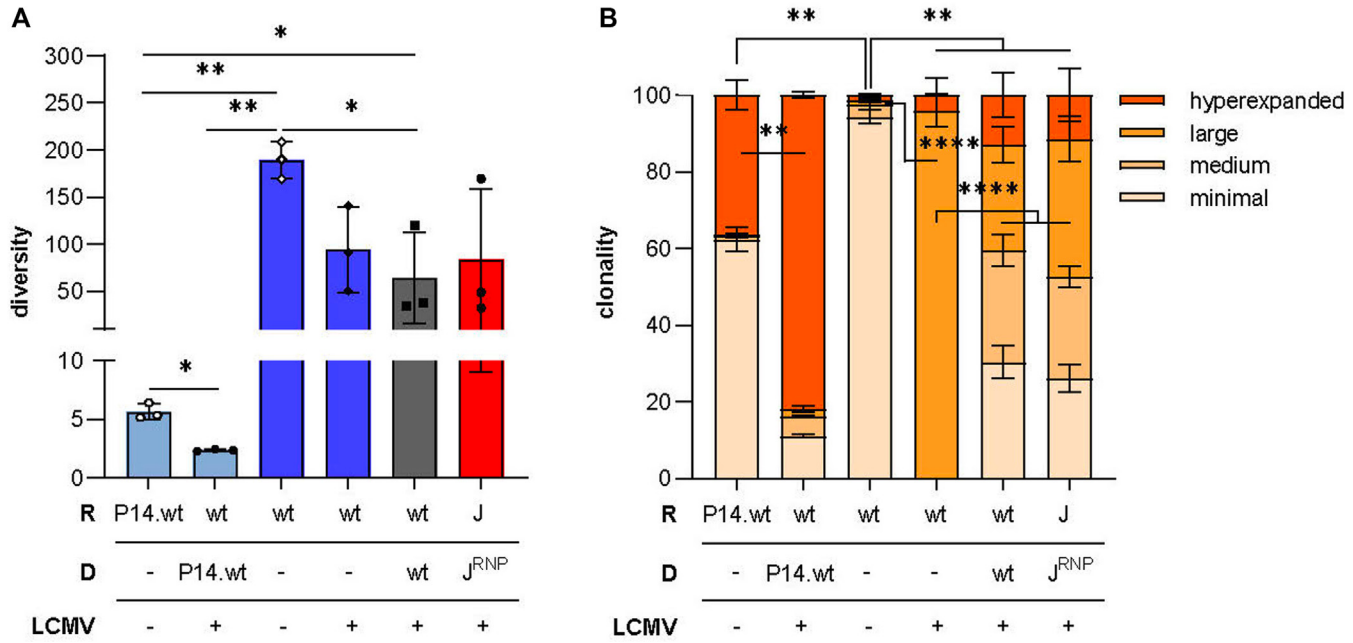

FIG 6. Analysis of TCR repertoire. **(A** and **B)** The TCRα/β repertoire was determined in 6 representative groups, as indicated (donor, recipient, +/− LCMV infection). Shown are diversity *(A)* and clonality *(B)* of the TCRα/β sequences. T-cell clones were grouped according to expansion as hyperexpanded ($0.01 < \times \leq 1$) *(dark orange)*, large ($0.001 < \times \leq 0.01$) *(orange)*, medium ($0.0001 < \times \leq 0.001$) *(light orange)*, and minimal ($0.00001 < \times \leq 0.0001$) *(beige)*. Mean values ± SD are depicted (n = 3 mice per group). Unpaired *t* test: $*P < .05$; $**P \leq .01$; $****P \leq .0001$. *D,* donor; *J, Jinx*; J^{RNP}, *Unc13d*-edited *Jinx* HSCs; *R,* recipient.

lentiviral insertional mutagenesis,[28,50] this example emphasizes the multiplicity of potential complications, which prompted us to assess gene editing-associated genotoxicity and potential clonal expansion in more detail. To mitigate genotoxicity, we identified CRISPR-Cas9 nucleases that combined high activity with high specificity.[40,51] The chosen double-hit strategy with 2 target sites in a protospacer-adjacent motif-in-in-configuration[52] led to excision of the cryptic splice site along with removal of the protospacer-adjacent motifs, thus improving editing efficiency, while preventing continuous re-cleavage of the genomic locus.[52,53] CAST-Seq and NGS analyses confirmed editing of >80% of *Unc13d* alleles in the absence of detectable off-target events. Immunophenotyping as well as indel distribution and TCR repertoire analyses confirmed the absence of apparent leukemogenesis or clonal expansion. Importantly, the indel distribution and the TCR diversity in mice transplanted with *Unc13d*-edited *Jinx* HSCs were comparable to wt recipient mice transplanted with wt HSCs. In all, these experiments addressed important translational questions: They confirmed multilineage reconstitution, including a functional restoration of $CD8^+$ T cells derived from *Unc13d*-edited HSCs and absence of signs of genotoxicity. This is consistent, for example, with preliminary safety data from ongoing clinical genome editing trials for sickle cell disease,[54] showing that CRISPR-Cas and base editing strategies can be used safely in the stem cell compartment. Furthermore, our data revealed tremendous heterogeneity of editing outcomes and suggest that indel distribution analysis can serve as a simple means to assess clonal expansion.

Disease-underlying mutations in FHL3 patients are found with about equal frequency in introns and the coding region of *UNC13D*.[55] Two-thirds of these mutations are point mutations, such as splice site mutations (35%), missense mutations (20%), and nonsense mutations (11%). A gene disruption approach would work to remove cryptic splice sites in introns, as done in this study. Additionally, base editing, and possibly prime editing, could be used to correct missense and nonsense mutations to restore translation of a functional MUNC13-4 protein. While theoretically possible, the design of mutation-specific gene editing tools is too laborious from a regulatory point of view. On the other hand, an all-in-one targeted integration strategy to correct all described mutations in *UNC13D* will be hampered to date by the inability to achieve sufficiently high gene targeting frequencies in long-term repopulating HSCs. While lentiviral *UNC13D* transfer has been successfully used to treat FHL3 in preclinical disease models,[22,45,46] much work remains to be done to achieve this goal with genome editing. Moreover, unless newborn screening is implemented, the majority of patients with FLH3 will have to be treated after HLH activation and remission induction.

mouse *(C)*. **(D-F)** Intraindividual indel distribution. BM samples (n = 3 mice, 8-10), split into lineage-negative *(dark red)* and lineage-positive *(red)* fractions, were subjected to NGS analysis. Shown are the proportions of edited *Unc13d* alleles *(D)*, the top 10 indel distributions within each fraction *(E)*, and Venn diagrams indicating the distribution of the top 1000 indel events among the 2 fractions *(F)*. *Bars (A* and *E)* depict mean values ± SD. Unpaired *t* test *(A)*, ns (not significant), $P > .05$. Lin^-, Lineage-negative; Lin^+, lineage-positive.

Follow-up studies will therefore also have to address whether HSC gene editing and transplantation of edited HSCs will work efficaciously in such a setting, too.

In sum, we developed a highly efficient gene editing protocol for murine HSCs, allowing us to edit 60% to 98% of *Unc13d* alleles *in vitro* and *in vivo*. Mice transplanted with *Unc13d*-edited HSCs developed a functional T-cell response with a polyclonal TCR repertoire, were able to clear LCMV infection, were protected from developing HLH, and did not show any evidence of therapy-induced complications, such as clonal outgrowth. Encouraged by this successful preclinical proof-of-concept study, we will develop further an HSC-based genome editing strategy to treat FHL3 in humans.

DISCLOSURE STATEMENT

This study was supported by the German Research Foundation (CRC 1160, projects A07, Z01 and Z02, to T.C., P.A., S.E., M.B., and C.S.), the German Federal Ministry of Education and Reserach (EkoEstMed–01ZZ2015 to G.A.), and a Mildred Scheel-professorship of the German Cancer Aid (DKH-70114112 to A.L.I.).

Disclosure of potential conflict of interest: T. Cathomen is an advisor to Cimeio Therapeutics, Excision BioTherapeutics, GenCC, and Novo Nordisk. T. Cathomen and T. I. Cornu have sponsored research collaboration with Cellectis and Cimeio Therapeutics, respectively. T. Cathomen, M. Boerries, and G. Andrieux hold a patent on CAST-Seq (US11319580B2). The rest of the authors declare that they have no relevant conflicts of interest.

We thank Hanspeter Pircher for P14-TCR transgenic mice, Katja Gräwe for technical support, the members of our laboratories for fruitful discussions and suggestions, and the Lighthouse Core Facility for help with flow cytometry (all Medical Center–University of Freiburg).

Key messages

- **Transplantation of genome-edited HSCs restores T-cell immunity in a murine disease model of FHL.**
- **Transplanted mice developed a polyclonal T-cell repertoire in the absence of signs of genotoxicity.**

REFERENCES

1. Pachlopnik Schmid J, Cote M, Menager MM, Burgess A, Nehme N, Menasche G, et al. Inherited defects in lymphocyte cytotoxic activity. Immunol Rev 2010;235:10-23.
2. Janka GE, Lehmberg K. Hemophagocytic syndromes—an update. Blood Rev 2014;28:135-42.
3. de Saint Basile G, Sepulveda FE, Maschalidi S, Fischer A. Cytotoxic granule secretion by lymphocytes and its link to immune homeostasis. F1000Res 2015;4:930.
4. Chinn IK, Eckstein OS, Peckham-Gregory EC, Goldberg BR, Forbes LR, Nicholas SK, et al. Genetic and mechanistic diversity in pediatric hemophagocytic lymphohistiocytosis. Blood 2018;132:89-100.
5. Bergsten E, Horne A, Hed Myrberg I, Arico M, Astigarraga I, Ishii E, et al. Stem cell transplantation for children with hemophagocytic lymphohistiocytosis: results from the HLH-2004 study. Blood Adv 2020;4:3754-66.
6. Wegehaupt O, Wustrau K, Lehmberg K, Ehl S. Cell versus cytokine-directed therapies for hemophagocytic lymphohistiocytosis (HLH) in inborn errors of immunity. Front Immunol 2020;11:808.
7. Heeg M, Ammann S, Klemann C, Panning M, Falcone V, Hengel H, et al. Is an infectious trigger always required for primary hemophagocytic lymphohistiocytosis? Lessons from in utero and neonatal disease. Pediatr Blood Cancer 2018;65:e27344.
8. Henter JI, Horne A, Arico M, Egeler RM, Filipovich AH, Imashuku S, et al. HLH-2004: diagnostic and therapeutic guidelines for hemophagocytic lymphohistiocytosis. Pediatr Blood Cancer 2007;48:124-31.
9. Mahlaoui N, Ouachee-Chardin M, de Saint Basile G, Neven B, Picard C, Blanche S, et al. Immunotherapy of familial hemophagocytic lymphohistiocytosis with antithymocyte globulins: a single-center retrospective report of 38 patients. Pediatrics 2007;120:e622-8.
10. Ehl S, Astigarraga I, von Bahr Greenwood T, Hines M, Horne A, Ishii E, et al. Recommendations for the use of etoposide-based therapy and bone marrow transplantation for the treatment of HLH: consensus statements by the HLH Steering Committee of the Histiocyte Society. J Allergy Clin Immunol Pract 2018;6:1508-17.
11. Merli P, Algeri M, Gaspari S, Locatelli F. Novel therapeutic approaches to familial HLH (emapalumab in FHL). Front Immunol 2020;11:608492.
12. Jordan MB, Hildeman D, Kappler J, Marrack P. An animal model of hemophagocytic lymphohistiocytosis (HLH): CD8+ T cells and interferon gamma are essential for the disorder. Blood 2004;104:735-43.
13. Fischer A, Blanche S, Neven B, Elie C, Picard C, de Saint Basile G, et al. Alemtuzumab as first line treatment in children with familial lymphohistiocytosis. Blood 2019;134:80.
14. Vallurupalli M, Berliner N. Emapalumab for the treatment of relapsed/refractory hemophagocytic lymphohistiocytosis. Blood 2019;134:1783-6.
15. Locatelli F, Jordan MB, Allen C, Cesaro S, Rizzari C, Rao A, et al. Emapalumab in children with primary hemophagocytic lymphohistiocytosis. N Engl J Med 2020;382:1811-22.
16. Marsh RA, Vaughn G, Kim MO, Li D, Jodele S, Joshi S, et al. Reduced-intensity conditioning significantly improves survival of patients with hemophagocytic lymphohistiocytosis undergoing allogeneic hematopoietic cell transplantation. Blood 2010;116:5824-31.
17. Gungor T, Teira P, Slatter M, Stussi G, Stepensky P, Moshous D, et al. Reduced-intensity conditioning and HLA-matched haemopoietic stem-cell transplantation in patients with chronic granulomatous disease: a prospective multicentre study. Lancet 2014;383:436-48.
18. Crozat K, Hoebe K, Ugolini S, Hong NA, Janssen E, Rutschmann S, et al. Jinx, an MCMV susceptibility phenotype caused by disruption of Unc13d: a mouse model of type 3 familial hemophagocytic lymphohistiocytosis. J Exp Med 2007;204:853-63.
19. Jessen B, Maul-Pavicic A, Ufheil H, Vraetz T, Enders A, Lehmberg K, et al. Subtle differences in CTL cytotoxicity determine susceptibility to hemophagocytic lymphohistiocytosis in mice and humans with Chediak-Higashi syndrome. Blood 2011;118:4620-9.
20. Gather R, Aichele P, Goos N, Rohr J, Pircher H, Kogl T, et al. Trigger-dependent differences determine therapeutic outcome in murine primary hemophagocytic lymphohistiocytosis. Eur J Immunol 2020;50:1770-82.
21. Weissert K, Ammann S, Kogl T, Dettmer-Monaco V, Schell C, Cathomen T, et al. Adoptive T cell therapy cures mice from active hemophagocytic lymphohistiocytosis (HLH). EMBO Mol Med 2022;14:e16085.
22. Soheili T, Durand A, Sepulveda FE, Riviere J, Lagresle-Peyrou C, Sadek H, et al. Gene transfer into hematopoietic stem cells reduces HLH manifestations in a murine model of Munc13-4 deficiency. Blood Adv 2017;1:2781-9.
23. Takushi SE, Paik NY, Fedanov A, Prince C, Doering CB, Spencer HT, et al. Lentiviral gene therapy for familial hemophagocytic lymphohistiocytosis type 3, caused by UNC13D genetic defects. Hum Gene Ther 2020;31:626-38.
24. Soheili T, Riviere J, Ricciardelli I, Durand A, Verhoeyen E, Derrien AC, et al. Gene-corrected human Munc13-4-deficient CD8+ T cells can efficiently restrict EBV-driven lymphoproliferation in immunodeficient mice. Blood 2016;128:2859-62.
25. Dettmer V, Bloom K, Gross M, Weissert K, Aichele P, Ehl S, et al. Retroviral UNC13D gene transfer restores cytotoxic activity of T cells derived from familial hemophagocytic lymphohistiocytosis type 3 patients in vitro. Hum Gene Ther 2019;30:975-84.
26. Biasco L, Rothe M, Buning H, Schambach A. Analyzing the genotoxicity of retroviral vectors in hematopoietic cell gene therapy. Mol Ther Methods Clin Dev 2018;8:21-30.
27. Nobles CL, Sherrill-Mix S, Everett JK, Reddy S, Fraietta JA, Porter DL, et al. CD19-targeting CAR T cell immunotherapy outcomes correlate with genomic modification by vector integration. J Clin Invest 2020;130:673-85.
28. Goyal S, Tisdale J, Schmidt M, Kanter J, Jaroscak J, Whitney D, et al. Acute myeloid leukemia case after gene therapy for sickle cell disease. N Engl J Med 2022;386:138-47.
29. Harper MT, van den Bosch MT, Hers I, Poole AW. Platelet dense granule secretion defects may obscure alpha-granule secretion mechanisms: evidence from Munc13-4-deficient platelets. Blood 2015;125:3034-6.
30. Chicka MC, Ren Q, Richards D, Hellman LM, Zhang J, Fried MG, et al. Role of Munc13-4 as a Ca2+-dependent tether during platelet secretion. Biochem J 2016;473:627-39.

31. Ramadass M, Catz SD. Molecular mechanisms regulating secretory organelles and endosomes in neutrophils and their implications for inflammation. Immunol Rev 2016;273:249-65.
32. Koch H, Hofmann K, Brose N. Definition of Munc13-homology-domains and characterization of a novel ubiquitously expressed Munc13 isoform. Biochem J 2000; 349:247-53.
33. Pircher H, Baenziger J, Schilham M, Sado T, Kamisaku H, Hengartner H, et al. Characterization of virus-specific cytotoxic T cell clones from allogeneic bone marrow chimeras. Eur J Immunol 1987;17:159-66.
34. Seki A, Rutz S. Optimized RNP transfection for highly efficient CRISPR/Cas9-mediated gene knockout in primary T cells. J Exp Med 2018;215:985-97.
35. Battegay M, Cooper S, Althage A, Banziger J, Hengartner H, Zinkernagel RM. Quantification of lymphocytic choriomeningitis virus with an immunological focus assay in 24- or 96-well plates. J Virol Methods 1991;33:191-8.
36. Kogl T, Muller J, Jessen B, Schmitt-Graeff A, Janka G, Ehl S, et al. Hemophagocytic lymphohistiocytosis in syntaxin-11-deficient mice: T-cell exhaustion limits fatal disease. Blood 2013;121:604-13.
37. Peake K, Manning J, Lewis CA, Barr C, Rossi F, Krieger C. Busulfan as a myelosuppressive agent for generating stable high-level bone marrow chimerism in mice. J Vis Exp 2015:e52553.
38. Kreutmair S, Erlacher M, Andrieux G, Istvanffy R, Mueller-Rudorf A, Zwick M, et al. Loss of the Fanconi anemia-associated protein NIPA causes bone marrow failure. J Clin Invest 2020;130:2827-44.
39. Illert AL, Albers C, Kreutmair S, Leischner H, Peschel C, Miething C, et al. Grb10 is involved in BCR-ABL-positive leukemia in mice. Leukemia 2015;29: 858-68.
40. Turchiano G, Andrieux G, Klermund J, Blattner G, Pennucci V, El Gaz M, et al. Quantitative evaluation of chromosomal rearrangements in gene-edited human stem cells by CAST-Seq. Cell Stem Cell 2021;28:1136-47.e5.
41. Mlambo T, Nitsch S, Hildenbeutel M, Romito M, Muller M, Bossen C, et al. Designer epigenome modifiers enable robust and sustained gene silencing in clinically relevant human cells. Nucleic Acids Res 2018;46:4456-68.
42. Ko A, Watanabe M, Nguyen T, Shi A, Achour A, Zhang B, et al. TCR repertoires of thymic conventional and regulatory T cells: identification and characterization of both unique and shared TCR sequences. J Immunol 2020;204:858-67.
43. Shugay M, Britanova OV, Merzlyak EM, Turchaninova MA, Mamedov IZ, Tuganbaev TR, et al. Towards error-free profiling of immune repertoires. Nat Methods 2014;11:653-5.
44. Nazarov V, Tsvetkov V, Rumynskiy EI. Bioinformatics Analysis of T-Cell and B-Cell Immune Repertoires [R package immunarch version 0.6.5]. 2020. Available at: https://www.semanticscholar.org/paper/Bioinformatics-Analysis-of-T-Cell-and-B-Cell-Immune-Nazarov-Tsvetkov/891049d2bdb1e8b70c2bf28c85392619e0a4f9a6. Accessed August 31, 2023.
45. Carmo M, Risma KA, Arumugam P, Tiwari S, Hontz AE, Montiel-Equihua CA, et al. Perforin gene transfer into hematopoietic stem cells improves immune dysregulation in murine models of perforin deficiency. Mol Ther 2015;23: 737-45.
46. Ghosh S, Carmo M, Calero-Garcia M, Ricciardelli I, Bustamante Ogando JC, Blundell MP, et al. T-cell gene therapy for perforin deficiency corrects cytotoxicity defects and prevents hemophagocytic lymphohistiocytosis manifestations. J Allergy Clin Immunol 2018;142:904-13.e3.
47. Felber M, Steward CG, Kentouche K, Fasth A, Wynn RF, Zeilhofer U, et al. Targeted busulfan-based reduced-intensity conditioning and HLA-matched HSCT cure hemophagocytic lymphohistiocytosis. Blood Adv 2020;4:1998-2010.
48. Bradford KL, Liu S, Krajinovic M, Ansari M, Garabedian E, Tse J, et al. Busulfan pharmacokinetics in adenosine deaminase-deficient severe combined immunodeficiency gene therapy. Biol Blood Marrow Transplant 2020;26:1819-27.
49. Majhail NS, Brazauskas R, Rizzo JD, Sobecks RM, Wang Z, Horowitz MM, et al. Secondary solid cancers after allogeneic hematopoietic cell transplantation using busulfan-cyclophosphamide conditioning. Blood 2011;117:316-22.
50. Jones RJ, DeBaun MR. Leukemia after gene therapy for sickle cell disease: insertional mutagenesis, busulfan, both, or neither. Blood 2021;138:942-7.
51. Jeong J, Jager A, Domizi P, Pavel-Dinu M, Gojenola L, Iwasaki M, et al. High-efficiency CRISPR induction of t(9;11) chromosomal translocations and acute leukemias in human blood stem cells. Blood Adv 2019;3:2825-35.
52. Lopez-Manzaneda S, Ojeda-Perez I, Zabaleta N, Garcia-Torralba A, Alberquilla O, Torres R, et al. In vitro and in vivo genetic disease modeling via NHEJ-precise deletions using CRISPR-Cas9. Mol Ther Methods Clin Dev 2020;19:426-37.
53. Song B, Yang S, Hwang GH, Yu J, Bae S. Analysis of NHEJ-based DNA repair after CRISPR-mediated DNA cleavage. Int J Mol Sci 2021;22:6397.
54. Zarghamian P, Klermund J, Cathomen T. Clinical genome editing to treat sickle cell disease—a brief update. Front Med (Lausanne) 2022;9:1065377.
55. Amirifar P, Ranjouri MR, Abolhassani H, Moeini Shad T, Almasi-Hashiani A, Azizi G, et al. Clinical, immunological and genetic findings in patients with UNC13D deficiency (FHL3): a systematic review. Pediatr Allergy Immunol 2021;32:186-97.

METHODS

Jinx reporter cell line

K562 cells (ATCC) were used to create a *Jinx* reporter cell line using a targeted integration strategy.[E1] Briefly, the *Unc13d* intron 26 sequence present in *Jinx* mice was inserted into position 146 of plasmid pEGFP-C1 (Clontech) via Gibson assembly[E2] to generate pEGFP-intron26-*Unc13d* that harbors homologous sequences to the *AAVS1* region. Integration into *AAVS1* was achieved by CRISPR-mediated knock-in (4D-Nucleofector, Lonza, SF-FF120). Limiting dilution under puromycin selection was used to produce single-cell clones.

REFERENCES

E1. Somarelli JA, Schaeffer D, Bosma R, Bonano VI, Sohn JW, Kemeny G, et al. Fluorescence-based alternative splicing reporters for the study of epithelial plasticity in vivo. Rna 2013;19:116-27.

E2. Gibson DG, Young L, Chuang RY, Venter JC, Hutchison CA 3rd, Smith HO, et al. Enzymatic assembly of DNA molecules up to several hundred kilobases. Nat Methods 2009;6:343-5.

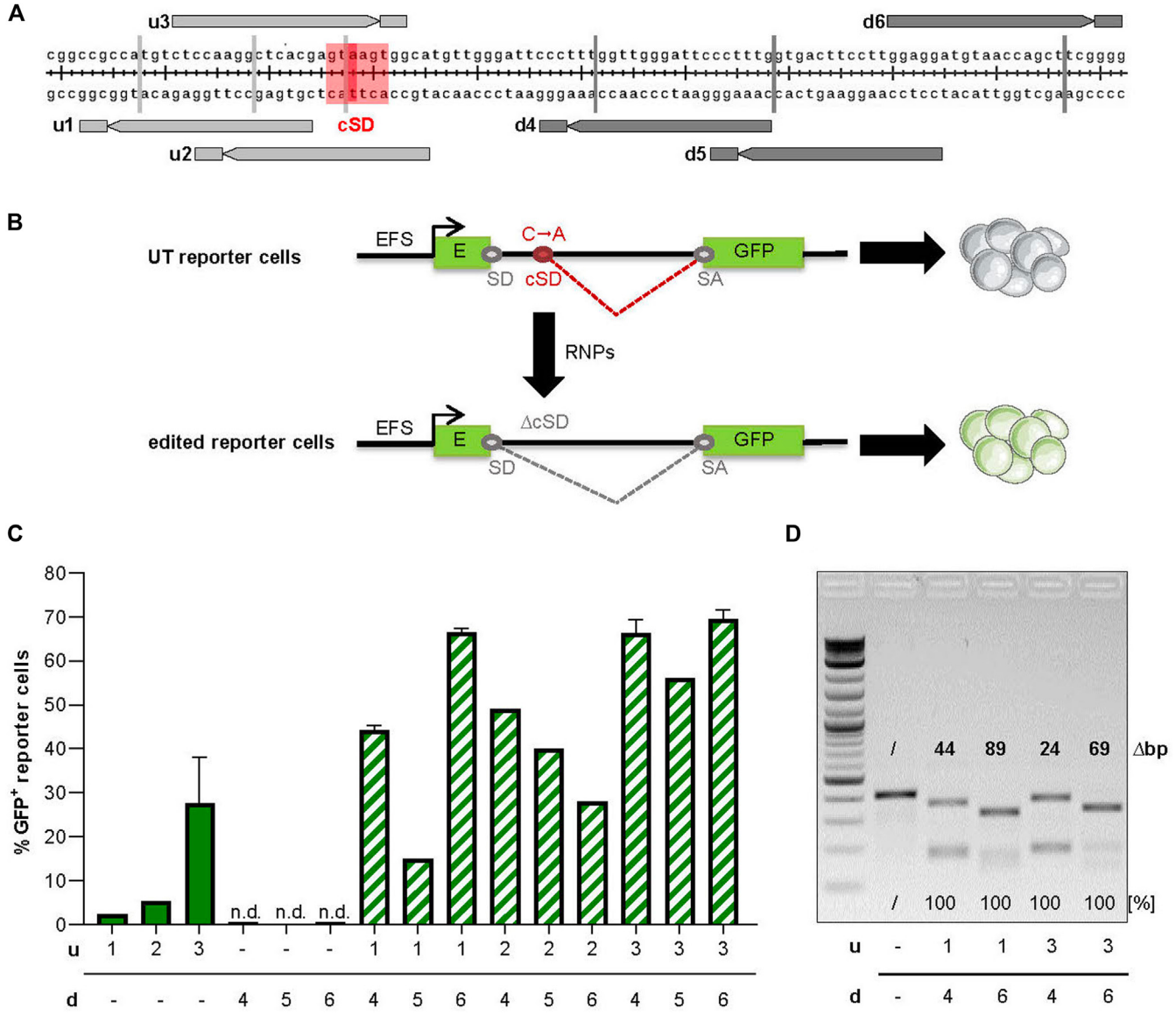

FIG E1. Initial evaluation of CRISPR-Cas nucleases. **(A)** Target sites in *Jinx* intron 26. The positions and sequences of 6 target sites of the CRISPR-Cas9 nucleases are indicated in *gray*, and the cryptic splice donor site is highlighted in *red*. **(B)** Schematic of the principle behind the *Jinx* reporter cell line. The reporter cells harbor an *EGFP* gene that is interrupted by *Jinx* intron 26 containing the C-to-A conversion that leads to aberrant splicing. Genome editing aims at disrupting or excising the cryptic splice donor site to restore correct splicing. **(C)** Functional correction. Fraction of GFP^+ cells was determined by flow cytometry after editing of reporter cells with CRISPR-Cas nucleases, either individually or by combining nucleases that target the cryptic splice donor site upstream and downstream. *Bars* depict either single or mean values ± SD. **(D)** Genotyping. T7E1 assay was performed on samples edited with the most promising combinations u1/d4, u1/d6, u3/d4, and u3/d6. The sizes (Δbp) of the perfect excision events as well as the percentages of T7E1-cleaved target amplicons are indicated. *cSD,* Cryptic splice donor site; d, downstream; *EFS,* elongation factor 1 alpha short promoter; *GFP,* green fluorescent protein; *n.d.,* not detectable; *u,* upstream.

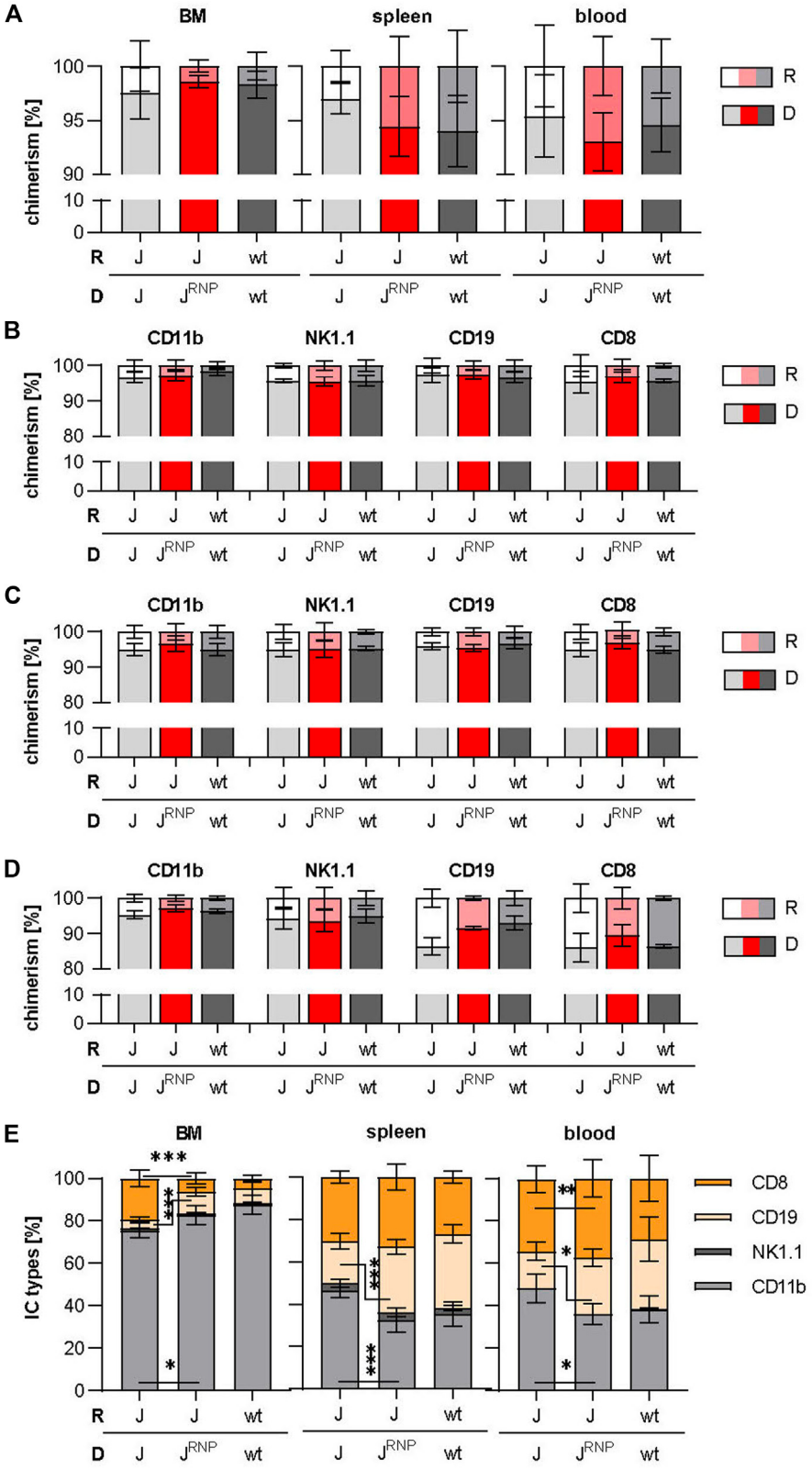

FIG E2. Evaluation of chimerism and immune cell subset distribution after stem cell transplantation. **(A-E)** BM, splenocytes and blood were assessed of the indicated groups after LCMV infection 14-34 weeks post-transplantation: donor, recipient, *Jinx*, *Unc13d*-edited *Jinx* HSCs, wt. Shown are the overall chimerism in BM, spleen, and blood *(A)* the percentages of graft-derived CD11b^{+}, NK1.1^{+}, CD19^{+}, and CD8^{+} immune cell types in BM *(B)*, spleen *(C)*, and blood *(D)*, as well as the fraction of immune cell types in those organs *(E)*. *Bars* depict mean values ± SD (n = 7-13 mice per group from 2-4 independent experiments with different donors and recipients). Unpaired *t* test: **P* < .05; ***P* ≤ .01; ****P* ≤ .001. *D,* Donor; *IC,* immune cell; *J, Jinx*; *J^{RNP}, Unc13d*-edited *Jinx* HSCs; *R,* recipient.

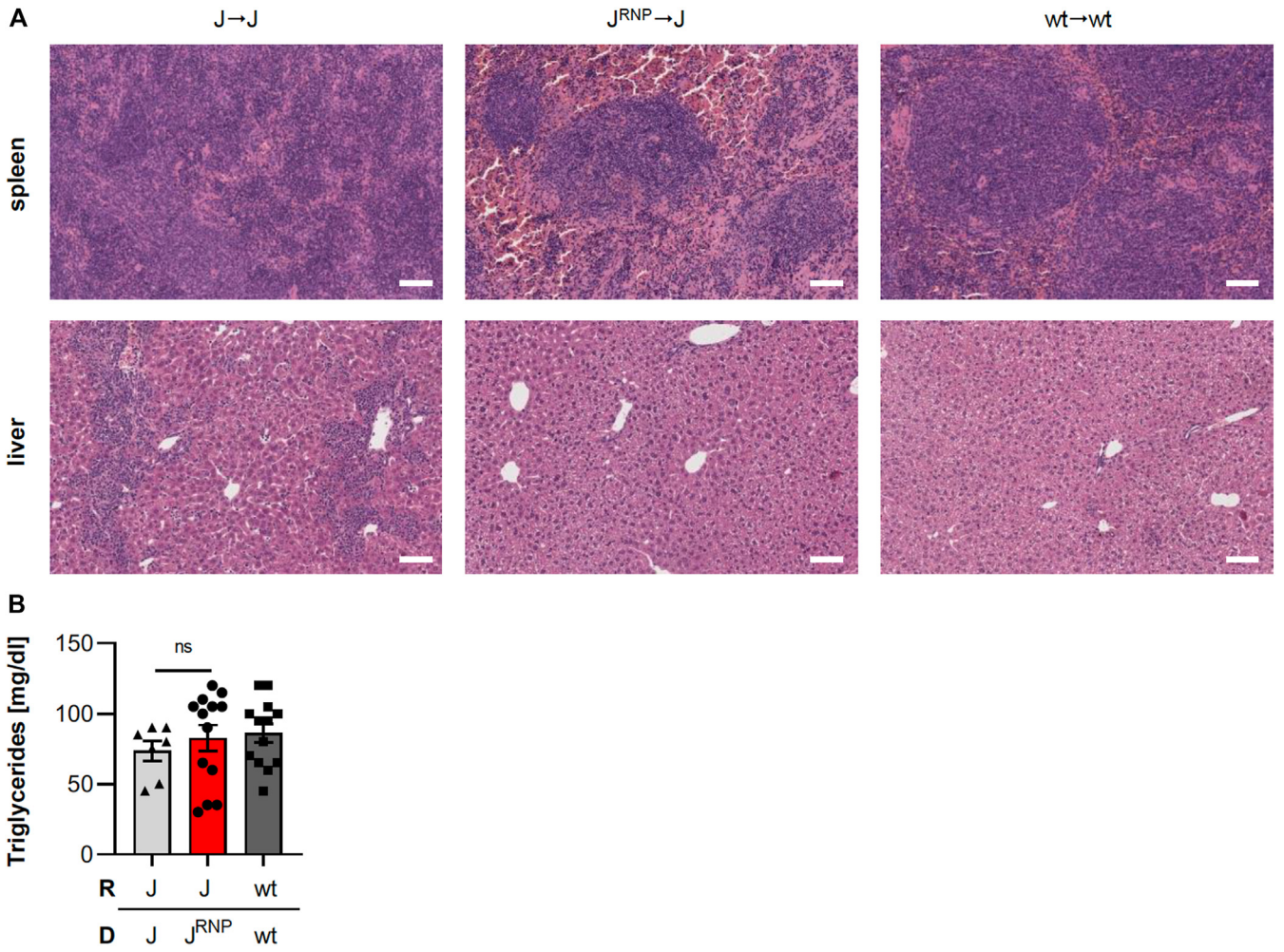

FIG E3. Hemophagocytic lymphohistiocytosis. **(A)** Histology. Representative hematoxylin and eosin staining of spleen and liver sections of transplanted mice 15 days after LCMV infection. Scale bar = 50 μm. **(B)** Serum concentration of triglycerides. *Bars* depict mean values ± SD (n = 7-13 mice per group from 2-4 independent experiments with different donors and recipients). Unpaired *t* test. ns (not significant), $P > .05$. *D,* Donor; *J, Jinx*; J^{RNP}*, Unc13d*-edited *Jinx* HSCs; *R,* recipient.

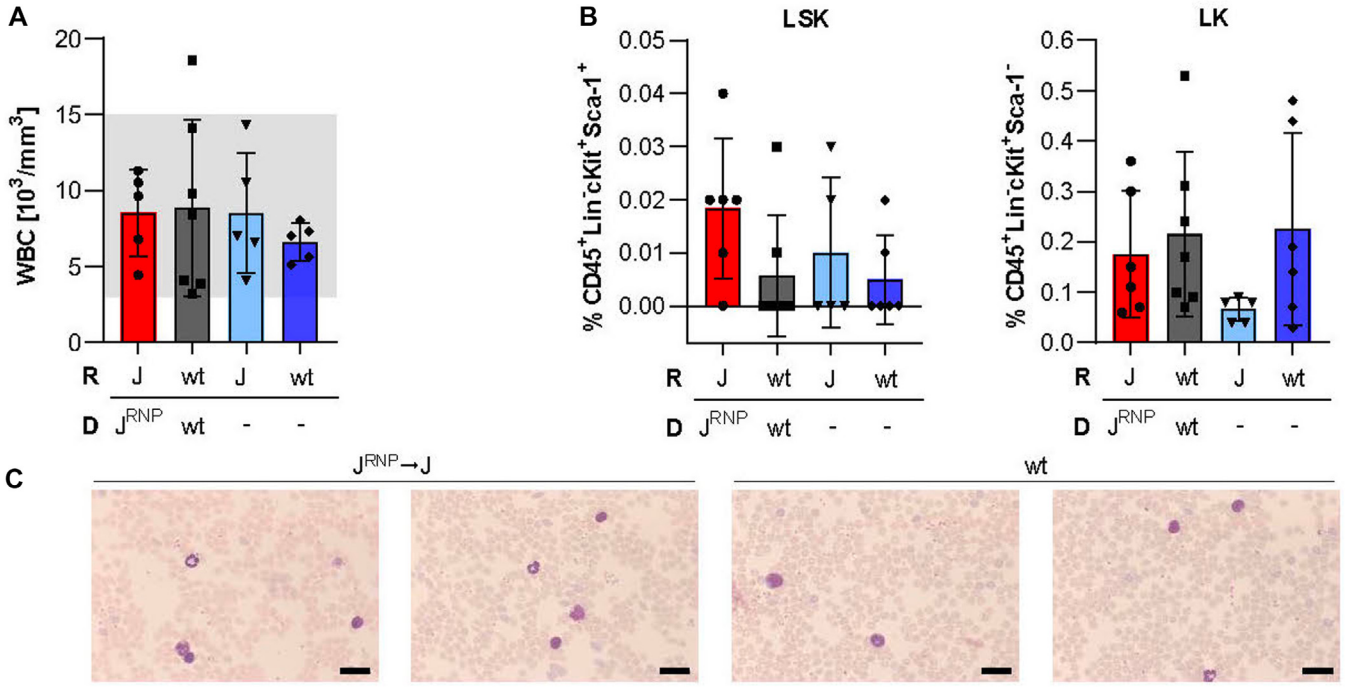

FIG E4. Immunophenotyping of peripheral blood before LCMV infection. Peripheral blood samples were analyzed 28-32 weeks post-transplantation before LCMV infection from different groups: donor, recipient, *Jinx*, *Unc13d*-edited *Jinx* HSCs, wt, nontransplanted (n = 5-7 from 2 experiments with different donors). **(A)** White blood cell count. The *gray area* defines the normal, nonleukemogenic white blood cell range. **(B)** Spectral flow cytometry analysis of $CD45^+Lin^-Sca\text{-}1^+cKit^+$ and $CD45^+Lin^-Sca\text{-}1^-cKit^+$ cells. **(C)** Blood smear analysis. Shown are representative Pappenheim-stained blood smears of 2 $J^{RNP}\rightarrow J$ and 2 untreated wt mice. Scale bars = 20 μm. −, nontransplanted; *D,* Donor; *J, Jinx*; *J^{RNP}, Unc13d*-edited *Jinx* HSCs; *LK,* $CD45^+Lin^-Sca\text{-}1^-cKit^+$; *LSK,* $CD45^+Lin^-Sca\text{-}1^+cKit^+$; *R,* recipient; *WBC,* white blood cell.

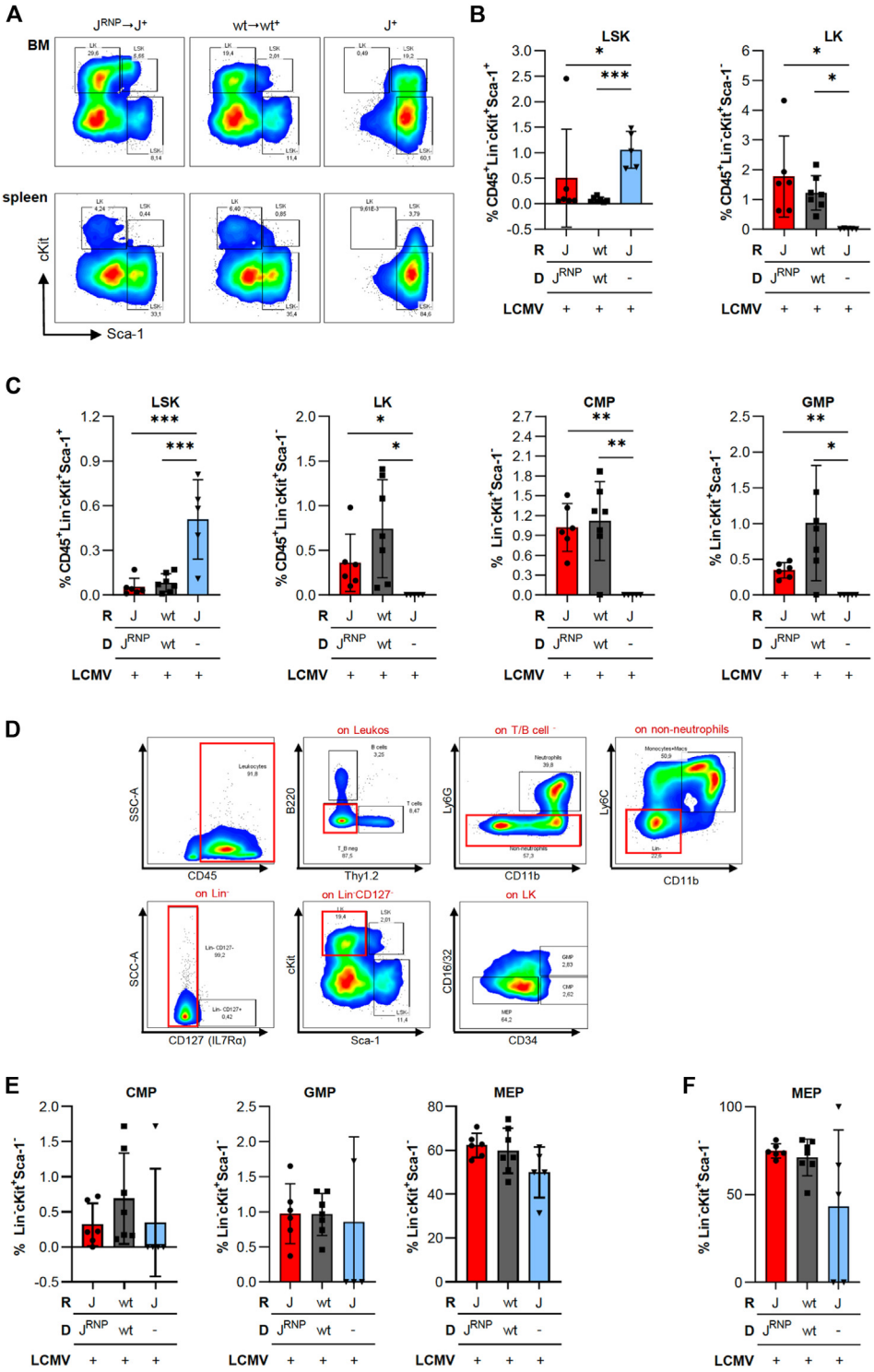

FIG E5. Immunophenotyping after infection with LCMV. BM and spleen samples of *Jinx* mice transplanted with *Unc13d*-edited HSCs *(red bars)* or wt mice engrafted with wt HSCs *(dark gray bars)* were harvested after LCMV infection 30-34 weeks post-transplantation (n = 5-7, 2 experiments with different donors). Nontransplanted, LCMV-infected *Jinx* mice *(light blue bars)* served as controls (n = 5, 2 experiments). **(A-F)** Assessment of hematopoietic precursor cell fractions. Shown are a representative flow cytometry analysis *(A)*; the percentages of $CD45^+Lin^-Sca\text{-}1^+cKit^+$ and $CD45^+Lin^-Sca\text{-}1^-cKit^+$ cells in BM *(B)* and the proportions of $CD45^+Lin^-Sca\text{-}1^+cKit^+$ cells, $CD45^+Lin^-Sca\text{-}1^-cKit^+$ cells, common myeloid progenitors, and granulocyte-monocyte progenitors in spleen *(C)*; representative spectral flow cytometry analysis to identify the proportions of common myeloid progenitors, granulocyte-monocyte progenitors, and megakaryocyte-erythroid progenitors *(D)*; percentages of CMP, GMP, and MEP in BM samples *(E)*; and the fraction of MEP in spleen samples *(F)*. *Bars* depict mean values ± SD. One-way analysis of variance and Mann-Whitney *U* test: $*P < .05$; $**P \leq .01$; $***P \leq 0.001$. −, Nontransplanted; *CMP,* common myeloid progenitors; *D,* donor; *GMP,* granulocyte-monocyte progenitors; *J, Jinx*; J^{RNP}, *Unc13d*-edited *Jinx* HSCs; *LK,* $CD45^+Lin^-Sca\text{-}1^-cKit^+$; *LSK,* $CD45^+Lin^-Sca\text{-}1^+cKit^+$; *MEP,* megakaryocyte-erythroid progenitors; *R,* recipient.

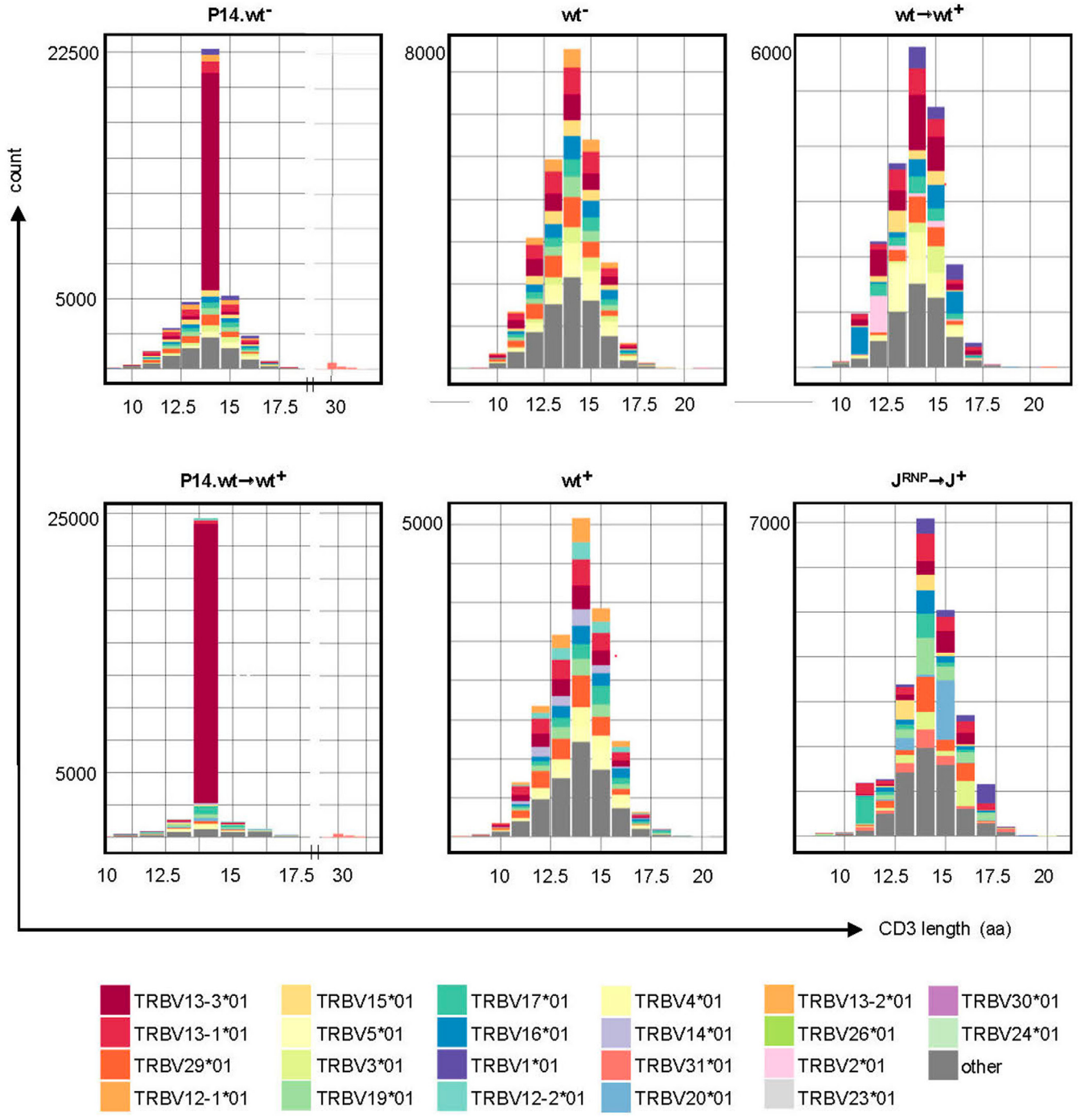

FIG E6. TCRα/β gene usage profile and CD3 lengths. Data was collected from 6 representative groups: noninfected P14.wt mice (P14.wt^{-}), LCMV-infected wt mice previously infused with P14.wt T cells (P14.wt→wt^{+}), noninfected (wt^{-}) and LCMV-infected (wt^{+}) wt mice, and wt mice grafted with wt HSCs (wt→wt^{+}) or *Jinx* mice grafted with *Unc13d*-edited HSCs (J^{RNP}→J^{+}) after LCMV challenge. Shown is one representative spectratyping plot per group. Key counts on the y-axis are plotted against the CD3 length in number of amino acids on the x-axis. The 22 identified dominant V regions are listed below the plots. Each colored segment represents a particular V region with a particular CD3 length. *Gray segments* represent all remaining regions that were present with low frequency. *aa,* Amino acids.

TABLE E1. Guide RNA sequences related to experimental procedures

Cleavage site	Guide ID	Direction	Sequences (5′-3′)	PAM
Upstream cSD	u1	rev	CGTGAGCCTTGGAG$^{\downarrow}$ACA	CGG
	u2	rev	TGCCACTTACTCGTGAG$^{\downarrow}$CCT	TGG
	u3	for	CTCCAAGGCTCACGAGT$^{\downarrow}$AAG	TGG
Downstream cSD	d4	rev	CAAAGGGAATCCCAACC$^{\downarrow}$AAA	GGG
	d5	rev	CCTCCAAGGAAGTCACC$^{\downarrow}$AAA	GGG
	d6	for	GGAGGATGTAACCAGCT$^{\downarrow}$TCG	GGG

cSD, Cryptic splice donor site; *d,* downstream; *for,* forward; *PAM,* protospacer-adjacent motif; *rev,* reverse; *u,* upstream.

TABLE E2. Flow cytometry antibodies related to experimental procedures

Staining	Antibody	Conjugate	Clone	Company, ID no.	Dilution
Chimerism	CD45.1	PE	A20	BD Biosciences, 561872	1:200
	CD45.1	AF700	A20	Biolegend, 110724	1:200
	CD45.1	BV510	A20	Biolegend, 110741	1:100
	CD45.2	FITC	104	eBioscience, 1-0454-82	1:200
	CD45.2	AF488	104	Biolegend, 109816	1:200
	CD45.2	BV785	104	Biolegend, 109839	1:100
In vitro assays and end point analyses	CD8a	APC	53-6.7	Invitrogen, 17-0081-81	1:100
	CD8a	BV510	53-6.7	Biolegend, 100752	1:200
	CD8a	PerCP-Cy5.5	53-6.7	Biolegend, 100734	1:400
	CD4	BV650	RM4-5	Biolegend, 100555	1:1000
	CD4	APC-Fire750	RM4-4	Biolegend, 116020	1:100
	CD11b	PE-Cy7	M1/70	Invitrogen, 25-0112-81	1:6000
	NK1.1	APC-Cy7	PK136	BD Pharmingen, 560618	1:400
	CD19	PB	6D5	Biolegend, 115523	1:100
	CD107A	PE	1D4B	Miltenyi Biotec, 130-102-219	1:100
	CD107A	PE	1D4B	Biolegend, 121612	1:50
	CD44	APC	IM7	Thermo Fisher Scientific, 17-0441-82	1:1000
	CD62L	BV650	MEL-14	Biolegend, 104453	1:1500
	KLRG1	PerCP-Cy5.5	2F1	Biolegend, 138418	1:150
	CD127	BV421	A7R34	Biolegend, 135027	1:100
	PD-1	BV785	J43	Biolegend, 135225	1:300
	PD-1	PerCP-Cy5.5	J43	Thermo Fisher Scientific, 46-9985-82	1:400
	Lag-3	PE-Cy7	C9B7W	Biolegend, 125226	1:100
	IFN-γ	APC	XMG1.2	Thermo Fisher Scientific, 17-7311-82	1:250
	TNF-α	AF488	MP6-XT22	Biolegend, 506313	1:100
	TCF1/7	AF488	C63D9	Cell Signaling, 6444S	1:100
	TOX	APC	TXRX10	Thermo Fisher Scientific, 50-6502-82	1:100
	CX3CR1	BV785	SA011F11	Biolegend, 149029	1:1000
	Tim-3	BV421	RMT3-23	Biolegend, 119723	1:100
	Dead cells	APC-Cy7	Zombie	Biolegend, 423106	1:1000

TABLE E3. Flow cytometry antibodies related to experimental procedures

Staining	Antibody	Conjugate	Clone	Company, ID No.	Dilution
HSC progenitors	CD45	PerCP-Cy5.5	30-F11	Thermo Fisher Scientific, 45-0451-82	1:1000
	Thy1.2	BV510	53-2.1	Biolegend, 140319	1:1000
	Ly6C	PE-Cy7	HK1.4	Thermo Fisher Scientific, 25-5932-82	1:1000
	Ly6G	PE-eF610	1AB-Ly6G	Thermo Fisher Scientific, 61-9668-82	1:1000
	B220	FITC	RA3-6B2	Thermo Fisher Scientific, 11-0452-82	1:1000
	CD11b	APC	M1/70	Thermo Fisher Scientific, 17-0112-82	1:1000
	Sca1 (Ly6A/E)	PE-Cy5	D7	Thermo Fisher Scientific, 15-5981-81	1:500
	CD117 (c-Kit)	APC-eFluor780	2B8	Thermo Fisher Scientific, 47-1171-82	1:500
	CD127 (IL-7Rα)	PE	A7R34	Thermo Fisher Scientific, 12-1271-82	1:500
	CD34	eFluor450	RAM34	Thermo Fisher Scientific, 48-0341-82	1:500
	CD16/32	sb600	93	Thermo Fisher Scientific, 63-0161-80	1:500

TABLE E4. Primers and program for *Unc13d* T7E1 and NGS analyses

Protocol	Primer ID	Direction	Sequences (5′-3′)	Program
T7E1/NGS PCR	Unc13d_Exon 26	for	TACATGAACACCAACCTGGTCC	98°C 3′; 9 cycles: [98°C 10″; 67°C 30″; 72°C 13″]
	Unc13d_Intron 26	rev	AGAGGAAGGAGATGCAGTTAGG	30 cycles: [98°C 10″; 67°C 30″; 72°C 13″]
				72°C, 7′; 4°C hold

Amplification using Q5 Hot Start High-Fidelity DNA Polymerase (New England BioLabs, M0493L).
for, Forward; *rev,* reverse.

TABLE E5. Primers and programs for *Unc13d* CAST-Seq analysis

Protocol	Primer ID	Direction	Sequences (5′-3′)	Program
PCRI	Unc13d_bait	for	CATGAACACCAACCTGG	95°C 5′; 12 cycles: [98°C 30″; 68°C 15″; 72°C 30″] 8 cycles: [98°C 30″; 62°C 15″; 72°C 30″] 72°C, 1′; 4°C hold
	Prey+linker (I)	rev	GTAATACGACTCACTATAGGGC	
	Unc13d_decoy (I)	rev	CTCCAAGGAAGTCACCAA	
	Unc13d_decoy (II)	for	GGGAGCTCACTGCTT	
PCRII	Unc13d_bait nested+linker	for	Gactggagttcagacgtgtgctcttccgatct CAACCTGGTCCAGGAGAACT	95°C 5′; 4 cycles: [98°C 30″; 72°C 15″; 72°C 30″] 16 cycles: [98°C 30″; 70°C 15″; 72°C 30″] 72°C, 1′; 4°C hold
	Prey+linker (II)	rev	ACACTCTACACTCTTTCCCTAC ACGACGCTCTTCCGATCTAGG GCTCCGCTTAAGGGAC	

Amplification using KAPA HiFi HotStart ReadyMix PCR Kit (Roche, KK2602).
for, Forward; *rev,* reverse.

TABLE E6. Primers and program for *Jinx* transcript quantification

Protocol	Primer ID	Direction	Sequences (5′-3′)	Program
ddPCR	Unc13d_Exon 25	for	CAAGGAGTCTGTTCTGCCCGA	95°C 5′; 40 cycles: [95°C 30″; 62°C 1′; ΔT 2°C/s] 4°C, 5′; 90°C 5′; 12°C hold
	Unc13d_Intron/Exon 26	rev	CTGCTGGGTACCTGCTGAAGTT	

Amplification using QX200TM ddPCRTM EvaGreen Supermix (BioRad, #1864034).
for, Forward; *rev,* reverse.

TABLE E7. Primers and programs for murine TCR repertoire library preparation

Protocol	Primer ID	Direction	Sequences (5′-3′)	Program
SmartScribe cDNA synthesis	SmartN	for	AAGCAGUGGTAUCAACGCAGAGUNNNNUNNNNUNNNNUCTTrGrGrG	72°C 3′; 42°C hold; 42°C 60′; 70°C 15′; 37°C hold; 37°C 20′; 4°C hold
	mTRAC1	rev	GGCGTTGGTCTCTTTGAAG	
	mTRBC1	rev	CACTTGTCCTCCTCTGAAAG	
PCR I	M1SS	for	AAGCAGTGGTATCAACGCA	98°C 3′; 18 cycles: [95°C 20″; 65°C 20″; 72°C 50″] 72°C 4′
	mTRAC2	rev	CGGCACATTGATTTGGGAG	
	mTRBC2	rev	TGTGGACCTCCTTGCCATTC	
PCR II	M1Sn_P7i7 (I)	for	tgactggagttcagacgtgtgctcttccgatctgactaccaCAGTGGTATCAACGCAGAG	98°C 3′; 18 cycles: [95°C 20″; 64°C 20″; 72°C 50″] 72°C 5′
	M1Sn_P7i7 (II)	for	tgactggagttcagacgtgtgctcttccgatctcagctaagCAGTGGTATCAACGCAGAG	
	M1Sn_P7i7 (III)	for	tgactggagttcagacgtgtgctcttccgatcttgctgttcCAGTGGTATCAACGCAGAG	
	M1Sn_P7i7 (IV)	for	tgactggagttcagacgtgtgctcttccgatctggtagtcaCAGTGGTATCAACGCAGAG	
	M1Sn_P7i7 (V)	for	tgactggagttcagacgtgtgctcttccgatctcattctcgCAGTGGTATCAACGCAGAG	
	M1Sn_P7i7 (VI)	for	tgactggagttcagacgtgtgctcttccgatctaagaccacCAGTGGTATCAACGCAGAG	
	mTRAC3_P5i5	rev	ACACTCTTTCCCTACACGACGCTCTTCCGATCTAGGTTCTGGGTTC TGGATG	
	mTRBC3_P5i5	rev	ACACTCTTTCCCTACACGACGCTCTTCCGATCTGGTGGAGTCACATT TCTCAG	

Amplification using Q5 Hot Start High-Fidelity DNA Polymerase (New England BioLabs, M0493L).
for, Forward; *rev,* reverse.